Summer 2005

Organization and signal processing of the descending tracts in the cervical spinal cord

Yanmei Tie
Louisiana Tech University

ORGANIZATION AND SIGNAL PROCESSING OF THE DESCENDING TRACTS IN THE CERVICAL SPINAL CORD

by

Yanmei Tie, B.E.

A Dissertation Presented in Partial Fulfillment
of the Requirements for the Degree
Doctor of Philosophy

COLLEGE OF ENGINEERING AND SCIENCE
LOUISIANA TECH UNIVERSITY

August 2005

APPROVAL FOR SCHOLARLY DISSEMINATION

The author grants to the Prescott Memorial Library of Louisiana Tech University the right to reproduce, by appropriate methods, upon request, any or all portions of this Dissertation. It is understood that "proper request" consists of the agreement, on the part of the requesting party, that said reproduction is for his personal use and that subsequent reproduction will not occur without written approval of the author of this Dissertation. Further, any portions of the Dissertation used in books, papers, and other works must be appropriately referenced to this Dissertation.

Finally, the author of this Dissertation reserves the right to publish freely, in the literature, at any time, any or all portions of this Dissertation.

Author Kai Ye

Date August 5, 2005

GS Form 14
(5/03)

ABSTRACT

This dissertation addresses the research for the development of spinal cord-computer interface (SCCI). The main objective of SCCI is to generate voluntary motor control signals for individuals with spinal cord injury (SCI).

In the neuroscience aspect, organization of the fibers in the descending tracts of the dorsolateral funiculus of the cervical spinal cord was investigated in cats. The spinal cord was penetrated with silicon substrate microelectrodes at 400 μm intervals in the medio-lateral direction at the C5/C6 and C6/C7 segmental borders. The stimulus consisted of a 20 ms train of charge-balanced biphasic pulses at 330 Hz. The evoked activities from selected forelimb muscles were acquired into computer. The muscle contractions were usually in the form of short twitches. In both segmental borders, the activation threshold was relatively higher in the middle of the dorsolateral funiculus. The majority of the muscles studied had a dorsal or ventral concentration of the activation points. The distal muscles were mostly activated in the ventro-lateral aspect of the funiculus, while the elbow muscle maps spread to both dorsal and ventral sides. These results show a functional organization in both cervical segments although there is an extensive overlap between the areas dedicated for each forelimb muscle.

In the neural signal processing aspect, the feasibility of increasing the channel separation for a neural interface was investigated using the blind source separation (BSS) technique. Multi-contact spinal cord recordings were assumed to be a linear mixture of

independent source signals inside the spinal cord. The results from simulated multi-channel recordings show a perfect channel separation. Further investigation was performed on real spinal cord recordings by eliminating the secondary sources, using the FastICA algorithm. The results suggest that the information rate of a spinal cord interface can be improved by separating the neural recordings into its independent components and selecting the ones with the largest distance between them. Comparison between ICA and PCA reveals that ICA is more suitable for this application.

This study constructs the first step in the development of SCCI. The results demonstrate that SCCI is feasible both in the neuroscience and signal processing perspectives.

LOUISIANA TECH UNIVERSITY

THE GRADUATE SCHOOL

August 1, 2005
Date

We hereby recommend that the dissertation prepared under our supervision by Yanmei Tie

entitled ORGANIZATION AND SIGNAL PROCESSING OF THE DESCENDING TRACTS IN THE CERVICAL SPINAL CORD

be accepted in partial fulfillment of the requirements for the Degree of Doctor of Philosophy in Biomedical Engineering

Supervisor of Dissertation Research

Head of Department
Biomedical Engineering
Department

Recommendation concurred in:

Advisory Committee

Approved:
Director of Graduate Studies

Approved:
Dean of the Graduate School

Dean of the College

GS Form 13
(5/03)

TABLE OF CONTENTS

ABSTRACT iii
LIST OF TABLES ix
LIST OF FIGURES x
ACKNOWLEDGMENTS xiii

CHAPTER 1. INTRODUCTION 1
1.1 Spinal Cord Injury (SCI) 1
1.2 Related Research 2
1.2.1 Functional Electrical Stimulation (FES) 2
1.2.2 Brain-Computer Interface (BCI) 3
1.3 Motivation 7
1.3.1 Spinal Cord-Computer Interface (SCCI) 7
1.3.1.1 Feasibility of SCCI 7
1.3.1.2 Advantages of SCCI 8
1.3.2 Organization of Descending Tracts 9
1.3.3 Separation of Multi-Channel Spinal Cord Recordings 11
1.3.4 Objectives 11
1.4 Impact of this Dissertation 12
1.5 Organization of this Dissertation 13

CHAPTER 2. BACKGROUND 15
2.1 Anatomy and Physiology of Spinal Cord 15
2.2 Descending Tracts 17
2.2.1 Corticospinal Tract (CST) 18
2.2.2 Rubrospinal Tract (RST) 19
2.3 Blind Source Separation (BSS) 19
2.4 Independent Component Analysis (ICA) 20
2.4.1 Definition of ICA 20
2.4.2 Assumptions and Ambiguities of ICA 21
2.4.3 Comparison between ICA and Principal Component Analysis (PCA) 21
2.4.4 ICA Algorithms 22
2.4.5 FastICA Algorithm 23

CHAPTER 3. METHODS 25
3.1 Experimental Set-up 25
3.1.1 Surgery Procedure 25
3.1.2 Instrumentation 27

3.1.2.1 Stimulation Electrode 27
3.1.2.2 Stimulation and Data Acquisition Software Developed Using LabVIEW 29
3.1.2.3 Stimulus Waveform 30
3.1.3 Stimulation and Data Acquisition Protocol 31
3.2 Data Analysis 34
3.2.1 Data Analysis of EMG Response 34
3.2.2 Two Normalization Procedures 35
3.2.3 Choice of Activation Threshold for Analysis 36
3.2.4 Data Plotting 37

CHAPTER 4. RESULTS AND DISCUSSION 38
4.1 Results 38
4.1.1 Raw EMG Signals 38
4.1.2 Muscle Activity Maps 40
4.1.3 Repertoire of Muscle Responses 45
4.1.4 Activation Thresholds 46
4.2 Discussion 48
4.2.1 Activation Maps 48
4.2.2 Observed Limb Movements 50
4.2.3 Concerns about the Signals and Instrumentation 51

CHAPTER 5. SEPARATION OF MULTI-CHANNEL RECORDINGS OF CORTICOSPINAL TRACT USING BLIND SOURCE SEPARATION METHOD 53
5.1 Methods 53
5.1.1 Data Collection 53
5.1.2 Simulation of Multi-Channel Spinal Cord Recordings 55
5.1.3 BSS Algorithm 57
5.1.4 Definition of Parameters 57
5.1.4.1 Signal-to-Noise Ratio (SNR) 57
5.1.4.2 Spatial Selectivity 58
5.1.4.3 Percent Crosstalk 59
5.2 Results 59
5.3 Discussion 64

CHAPTER 6. SEPARATION OF SPINAL CORD MOTOR SIGNALS USING FASTICA ALGORITHM 66
6.1 Methods 66
6.1.1 Data Collection 66
6.1.2 Data Analysis 66
6.1.2.1 Definition of Trials, Recordings, and Acquisitions 66
6.1.2.2 Data Preprocessing Using PCA 66
6.1.2.3 Separation of Independent Sources Using FastICA Algorithm 68
6.1.2.4 Statistical Analysis Based on MANOVA Test 70

6.2 Results 71
6.3 Discussion 75

CHAPTER 7. CONCLUSIONS AND FUTURE RESEARCH 80
7.1 Conclusions 80
7.2 Future Research 82

APPENDIX A: STIMULATION AND DATA ACQUISITION SOFTWARE DEVELOPED USING LABVIEW 84

APPENDIX B: FLOWCHART OF EMG RESPPONSE ANALYSIS 88

REFFERENCES 90

LIST OF TABLES

Table 2.1 Comparison between ICA and PCA 22

Table 3.1 Six groups of forelimb muscles and their abbreviations 27

Table 4.1 Number of muscles being recorded during each experiment 42

Table 4.2 Activated muscle movements other than the ipsilateral forelimb muscles 45

Table 5.1 The percent crosstalk measurements 64

Table 6.1 Correlation coefficients between the mixed signals and the reconstructed projections of the four separated sources for each contact 72

Table 6.2 Alpha values of the MANOVA test 75

LIST OF FIGURES

Figure 1.1 Examples of intracortical electrode arrays under development. (a) Silicon 100 electrode array; each is separated by 400 μm. (b) Silicon array shown against a common scale to illustrate the size of these devices. (c) Polyamide "bioactive electrode" array. (d) Michigan thin film 256-shank array of 1024 multiplexed sites with mounted signal processing electronics 5

Figure 1.2 Somatotopic organization in the cat motor cortex 10

Figure 2.1 Segmental organization of the spinal cord 16

Figure 2.2 The two pathways of the spinal cord 16

Figure 2.3 Cross section of the spinal cord showing descending and ascending tracts 17

Figure 2.4 Diagram of the corticospinal tract 18

Figure 3.1 Pictures of cat forelimb muscles (refer to Table 3.1 for muscle abbreviations). (a) Lateral aspect of forearm: 1. LoTriC; 2. LaTriC; 3. Bra; 4. BraR; 5. ECRL; 6. ECRB; 7. EDC; 8. EDL; 9. ECU; 10. FCU. (b) Medial aspect of forearm: 1. BraR; 2. ECRL; 3. ECRB; 5. FCR; 6. PL; 7. FCU; 8. Cdel; 9. Bi; 11. LoTriC 26

Figure 3.2 Single shank Michigan probe and its parameters 28

Figure 3.3 (a) PC board. (b) Probe tip of the single shank 16-channel Michigan electrode 29

Figure 3.4 Stimulus waveform showing a charge-balanced cathodic first biphasic current pulse 31

Figure 3.5 Diagram of the cross-section of C5/C6 segmental border showing the scanned area 33

Figure 3.6 Histology picture of a slice taken at C5/C6 segmental border showing the electrode cleft 34

Figure 3.7 The starting and ending points of the activity marked manually to calculate the EMG strength 35

Figure 4.1 Muscle activities recorded from five representative forelimb muscles following a 20 ms stimulation train at 330 Hz 39

Figure 4.2 EMG strengths of three different muscles during a trial of 16 consecutive trains 40

Figure 4.3 The normalized EMG strengths maps for each forelimb muscle separately on the dorsolateral funiculus at the C5/C6 segmental border of the spinal cord in one cat 41

Figure 4.4 The normalized EMG strengths combined from all cats and mapped onto the spinal cord for each muscle individually at C5/C6 segmental border 43

Figure 4.5 The normalized EMG strengths combined from all cats and mapped onto the spinal cord for each muscle individually at C6/C7 segmental border 44

Figure 4.6 The average of stimulation current thresholds mapped on the dorsolateral funiculus of C5/C6 segmental border 47

Figure 4.7 The average of stimulation current thresholds mapped on the dorsolateral funiculus of C6/C7 segmental border 47

Figure 5.1 Multi-contact electrode designs used for epidural and intradural recordings from the LCST 54

Figure 5.2 Extraction of the motor components from the spinal cord signals using stimulus-trigger averaging (n = 256) 55

Figure 5.3 The signal flow diagram of this study 56

Figure 5.4 256 consecutive acquisitions of six neural patterns before averaging (with stimulus artifacts removed) 60

Figure 5.5 Stimulus-trigger averaged source patterns 61

Figure 5.6 Averaged version of the simulated multi-contact neural recordings 61

Figure 5.7 Learning trajectory of the BSS neural network coefficients ($\boldsymbol{W}$) of the first data set, showing convergence 62

Figure 5.8 Neural patterns at the BSS neural network output 63

Figure 6.1 A depiction of the neural sources inside the lateral corticospinal tract (dotted area) and how they superimpose at the recording contacts 68

Figure 6.2 The block diagram of how the FastICA algorithm was applied to obtain the estimated source signals from the observed multi-contact neural recordings 69

Figure 6.3 An example of the averaged version of the 4-contact recordings (mixed signals), overlaid by the projections of the four sources that generate the mixture 72

Figure 6.4 The plot of the "primary source column" of mixing matrix $\boldsymbol{A}$ of three recordings of an example trial. Each plot is shifted slightly to the right for clarity of the figure 73

ACKNOWLEDGMENTS

First, I would like to extend my sincere gratitude to my chair advisor, Dr. Mesut Sahin, for his understanding, encouraging, and personal guidance in my pursuit of Ph.D. degree in Biomedical Engineering. I have learned a lot not only from his broad knowledge in engineering and science, but also from his conscientious, industrious, and enthusiastic attitude toward scientific research. His deep insights on scientific problems and his perseverance encourage me all the time.

I am deeply grateful to my committee members, Dr. Charles Robinson, Dr. Walter Besio, Dr. Stanley Cronk, and Dr. Raja Nassar. They have provided generous advice, assistance, and valuable feedback throughout this work. I also would like to thank all the professors who have taught me during my graduate study at Louisiana Tech University. The members in the Neural Engineering Laboratory in Center for Biomedical Engineering and Rehabilitation Science have helped me a lot. I thank them very much.

Most importantly, I would like to express my tremendous love and heartfelt gratitude to my entire family for their endless love, dedication, patience, and belief in me during these years. They are my father, Jingxiang Tie, my mother, Shuqin Wan, my husband, Yuan Shang, my two older brothers, Weiquan Tie and Weishun Tie, my sister-in-laws, Hongyan Dai and Hong Li, and my two lovely nieces, Yi Tie and Ziyun Tie. To study abroad and live alone is the most drastic change in my life. It has been a long journey to achieve the Ph.D. degree, and I was not fully prepared for the difficulties that I

have encountered during this period. It is because of the untiring love, support, and encouragement from my dear family that I could survive the culture shock, overcome all the difficulties, and persist in my career pursuit. I owe a lot to my entire family, especially my parents and my husband. My achievement belongs to all my family members. They deserve full credit for it. I am also very thankful to my parents-in-law. They have been very supportive.

One of the best experiences during these years is the birth of my precious little daughter, Emily Erwen Shang, who has accompanied and grown with me for the last year of my Ph.D. study and provided an additional and joyful dimension to our life mission. She is a sweet and bright hope for the future.

Finally, this research was financially supported by a Biomedical Engineering Research Grant from The Whitaker Foundation (RG-01-0366). The preliminary work was supported by a grant from Christopher Reeve Paralysis Foundation (SB1-9909-2). The single shank Michigan probes were fabricated by the Center for Neural Communication Technology (CNCT) at the University of Michigan.

CHAPTER 1

INTRODUCTION

1.1 Spinal Cord Injury (SCI)

Spinal cord injury (SCI) is damage to the spinal cord caused by trauma or disease. The annual incidence of SCI is approximately 11,000 new cases in the United States. The number of people with SCI in the United States today is between 222,000 and 285,000. The majority of SCI patients (78.2%) are males and the average age at injury is 38.0 years [1].

SCI results in a wide variety of motor disabilities, depending on the level and degree of damage. The skeletal muscles distal to the point of damage become paralyzed due to disrupted neural conduction. Generally speaking, the higher in the spinal column the injury occurs, the more dysfunction will occur. There are two types of SCI, complete and incomplete. In a complete injury, there is no any function (sensation and voluntary movement) below the level of the injury and both sides of the body are equally affected. However, a patient with incomplete SCI may have some functioning below the primary level of the injury, and the influence of the injury on the left and right sides of the body may be different. Incomplete SCI is becoming more common due to the advances in acute treatment of SCI.

In the high-level SCI, quadriplegia, which results from cervical injuries, the voluntary motor control is severely limited. The life expectancies of SCI patients continue to increase although they are still somewhat below that of the persons without SCI. However, the cost of taking care of SCI patients is extremely high. The lifetime health care and living expense for a person who has suffered SCI since 25 years old is estimated as over two million dollars [1]. Thus there is a great need for a method that can partially substitute the lost voluntary motor control for the individuals with SCI. The devices that aim to substitute for the control of body functions that have been impaired by neurological damage are called neural prostheses.

1.2 Related Research

There have been advances in the acute treatment of SCI to minimize physical damage and preserve neurological functions over the past few years [2]. However, the treatment of chronic SCI remains a great challenge. Among research for treatment of chronic SCI and its complications, functional electrical stimulation (FES) and brain-computer interface (BCI) are two main areas.

1.2.1 Functional Electrical Stimulation (FES)

Functional electrical stimulation (FES) is the use of transcutaneous electrical current to initiate contractions in paralyzed extremities as a form of therapeutic treatment of SCI or other neuromuscular illnesses. FES has been used to electrically activate the lower motor neuron and the muscle it controls to restore the lost limb functions in SCI, such as hand grasp, standing and walking. The electrical stimulation is applied either by skin surface electrodes or by implanted electrodes. Three main applications for FES have

been developed over the past decade: FES for function of upper extremity (hand or arm), FES for function of lower extremity (leg), and FES for exercise.

The current upper extremity FES system use a single-channel proportional control signal (a shoulder joystick) to control the intensity of the electrical currents applied to the target muscles to provide a hand grasp function [3]. There is also an ongoing effort to use EEG signals as a command signal for this purpose [4].

Several FES systems have been commercially available. The Parastep System is a microcomputer-controlled non-invasive FES system that offers 4 or 6 channels of skin electrode stimulation to allow standing and limited walking [5]. The Freehand System developed by Case Western Reserve University is the world's first surgically implanted device to restore movement to a paralyzed limb thus gives high quadriplegic patients hand function [6]. It includes surgically implanted components and a controller that is worn externally. The system has been approved by the Food and Drug Administration (FDA). The cost of such a system is about $50,000, much less compared with the lifetime expense of a person with quadriplegia.

However, FES has some major problems, such as a low information rate less than 25 bits/min, rapid fatigue of artificially stimulated muscles, poor control of complex neuromuscular system, and large requirement of attention to control the system due to the unnatural man-machine interface.

1.2.2 Brain-Computer Interface (BCI)

Over the past decade, a number of brain-computer interface (BCI) methods have been proposed. These programs concentrate on developing radically new control and communication technology for those with severe neuromuscular disorders, such as SCI,

amyotrophic lateral sclerosis, and brainstem stroke. BCI provides the users with basic control and communication capabilities that do not depend on peripheral nerves and muscles.

Like any communication and control system, a BCI system has an input, output and translation algorithm that converts input to output. Current BCI converts electrophysiological input, such as user-initiated or evoked changes in EEG or cortical single-neuron activity, into output signals that control external devices.

There are mainly two broad categories of BCI devices, noninvasive and invasive. Noninvasive methods convert electrophysiological input, such as electroencephalography (EEG) [7, 8] or event-related potentials (ERPs) [9, 10] signals recorded from the scalp, into output that controls external devices. Paralyzed subjects can move a cursor on a computer screen or to indicate discrete choices using such systems [11]. However, the maximum information transfer rate of current EEG-based BCI is only 5-25 bit/min [12], which is far from generating signals that can be used to control a wheelchair or a robot arm. Moreover, extensive training and great concentration from the users are required to generate these signals.

Invasive approaches of BCI use intracortical recordings to capture the action potentials of many individual neurons, thus require implantation of multiple metal electrodes on the cortical surface or, single wire, cone, or microelectrode arrays inserted into the cortex [13-17]. Cone electrodes have provided stable single-unit recordings in primates (including human) for several years [18]. The information rate is similar to that of scalp EEG methods due to the limitation on the number of cone electrodes that can be

implanted. More advanced microelectrode arrays have been developed (Figure 1.1 [19]), which are necessary for successful multiple neuron recordings in human subjects.

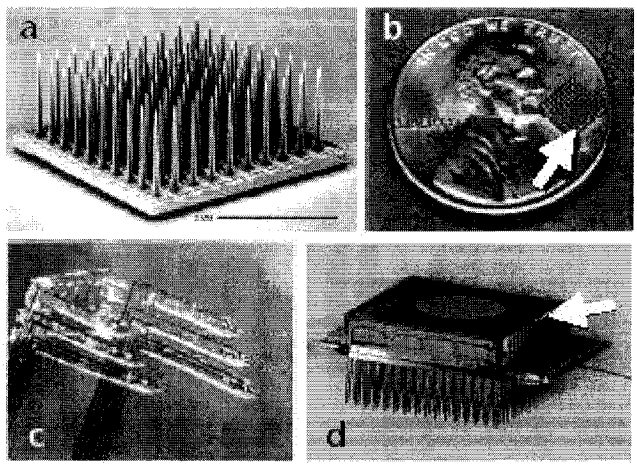

Figure 1.1 Examples of intracortical electrode arrays under development.
(a) Silicon 100 electrode array; each is separated by 400 μm.
(b) Silicon array shown against a common scale to illustrate the size of these devices.
(c) Polyamide "bioactive electrode" array.
(d) Michigan thin film 256-shank array of 1024 multiplexed sites with mounted signal processing electronics.

It has been demonstrated that hand trajectory can be recovered from the activity of populations of neurons in the motor cortex [20-22]. The advances in mathematical techniques make it possible that the brain output connected to robot arms or computer cursors can mimic a monkey's ongoing arm movements as they occur. This result suggests that the neural decoding of such systems that use intracortical implantation of multi-electrode array is fast and accurate. However, these control signals are far from producing the full repertoire of arm movements. Furthermore, more electrode arrays are needed to provide more complex actions or simultaneous control of multiple body parts [19]. Recent work also demonstrates that cortically derived command signals can

substitute for hand motion in behavioral task [20, 21]. Monkeys could move a cursor to a target displayed on the screen by command signals obtained from the neuronal activity recorded from the cortex with microelectrode arrays.

Currently, BCI is still in its infancy. It requires major surgery and bulky equipment [23]. Researchers seem in favor of the devices based on intracortical recordings since they can obtain individual action potential from multiple cells and possibly relay more complex information that can be used for more complex tasks.

Although the approach of applying microelectrode arrays in the pre-motor and motor cortical areas for BCI is promising, there are still some limitations with this method due to its attempt to chronically record from single cells. The limitations include the following:

- The population of cells recorded will change day to day because nerve cells migrate with respect to the tip of the electrode, and thus the computer algorithm of extraction of the voluntary motor signals needs to be continuously modified.
- It is very difficult to identify a cell by the shape of the action potential it generates since action potentials from different cells look very much alike, which makes it a challenge to keep track of a cell.
- Only a small portion of motor cortex cells involved in upper limb control can be sampled due to a number of limitations, such as the limited number of electrodes that can be placed in a unit area of the array, the low yield on the percentage of electrodes that actually record from a nerve cell, and the limitation on the percutaneous connections.

1.3 Motivation

1.3.1 Spinal Cord-Computer Interface (SCCI)

An alternative approach to generate the voluntary command signal for the people with SCI is to record the descending motor signals from the intact portion of the cervical spinal cord above the injury. The extracted motor signals can be used to control an upper limb neural prosthesis or a wheelchair for the individuals with SCI. This neural interface is called spinal cord-computer interface (SCCI).

1.3.1.1 Feasibility of SCCI

From the functional anatomy of the spinal cord, we know that three descending motor control pathways originate in the motor cortex of the frontal lobe: lateral corticospinal tract (LCST), ventral (or anterior) corticospinal tract (VCST) and corticobulbar tract. The corticobulbar tract primarily bilaterally innervates motor neurons of the brainstem and is responsible for activating cranial nerve motor neurons. Besides LCST, the rubrospinal tract (RST) is another important pathway for voluntary motor control. The fibers of the LCST and the RST become close to the surface below medulla in the white matter and occupy a large portion of the dorsolateral funiculus of the cervical spinal cord. Epidural recording of the corticospinal activity evoked by transcranial electrical stimulation has been used for cord trauma assessment during spinal surgery [24-28]. Therefore, the electrodes can be implanted on the surface or within the spinal cord to record the neural signals from descending tracts.

The distal portion of the upper motor neuron goes through "Wallerian degeneration (WD)" after injury [29]. However, the time course of the retrograde degeneration [30-32] for the proximal part of the axons is much slower, and a significant

portion of the fibers is preserved even years after injury [33, 34]. Therefore, to record the descending motor signals from the intact portion of the cervical spinal cord above injury is feasible.

1.3.1.2 Advantages of SCCI

The main difference between SCCI and BCI is the source of the voluntary motor control signals. Compared with the cortical approaches, obtaining the voluntary motor signals from the spinal cord has many potential advantages:

- Unlike the motor cortex, the LCST and the RST contain only motor fibers closely packed together. Thus the amount of contaminating signal should be minimized. Signal processing to extract the motor signals is expected to be less than that of the cortical approaches. Note that the spinal cord recording from the SCI subjects will not contain the afferent signals since the afferent fibers are severed by the injury.
- Unlike the motor cortex, all the tract fibers are oriented in the same direction longitudinally, which allows the summation of extraneural potentials to be recorded.
- Since there are more than a million fibers in the LCST in humans [35], a small fraction of the tract fibers should be enough to generate signals that can be recorded from the spinal cord surface or within it.
- Since the ensemble of the neural activity from an axon population with similar functions (not the individual action potentials) will be recorded, the recordings should not be as sensitive to the distance between the electrode and the active fibers as in the cortical approaches.

- The implantation site may be more acceptable to the subjects compared to the cortical approach.
- From a rehabilitation perspective, SCI patients with SCCI can actively use the descending motor fibers to improve the preservation of severed axons due to activity dependent preservation of neuronal circuits found in many parts of the central nervous system (CNS).

1.3.2 Organization of Descending Tracts

The somatotopic organization of the LCST fibers as they descend in the dorsolateral white matter was assumed to exist based on clinical observations of spinal cord trauma patients and depicted in many neuroanatomy books. However, the evidence from the animal experiments does not support such an organization. A number of groups have investigated the somatotopic organization of the LCST and RST fibers and their terminations in the gray matter [36-41], primarily in monkeys and cats using the classical axon tracing methods. In general, the somatotopic organization of the motor cortex was used as the reference point to study the organization in the LCST or the pyramidal tract. These neuroanatomical studies concluded that the somatotopic organization that exists in the pyramidal tract is irreversibly lost below the level of pons, and there is no somatotopic organization in the LCST as it descends in the white matter of dorsolateral funiculus of the spinal cord. Similar to the LCST, a functional organization, at the origin of RST, within the medullary reticular formation, was found to exist by microstimulation in the unanesthetized cats [42, 43]. However, there is no study of whether the fibers of the descending tracts have any organization with respect to the limb function, within the white matter of the spinal cord.

It has been shown that there is a strong somatotopic organization in the motor cortex (Figure 1.2 [44]). However, information of the direction and force of the limb movements are determined by "population coding", not by individual cells [45, 46]. How the population coding is translated into limb movements is determined by the connections between the motor cortex and the various spinal segments. Individual LCST fibers give out multiple collaterals to various spinal cord segments [47]. A group of LCST terminate in the propriospinal neurons located in the layer VII of the C3-C4 segments, which terminate in the cervical enlargement and play an important role in mediating the forelimb control [37, 48]. These evidences suggest that it is impossible for a one-to-one mapping, between the pyramidal cells of the primary motor cortex and the LCST fibers in the white matter of the spinal cord, to exist. Moreover, there are several other fiber tracts descending from higher centers that comprise at least 40 % of the corticospinal tract (CST) [49]. Therefore, instead of studying the organization within the LCST in relation to the primary motor cortex using histological methods, the organization of LCST needs to be studied with respect to the limb function using electrophysiological methods.

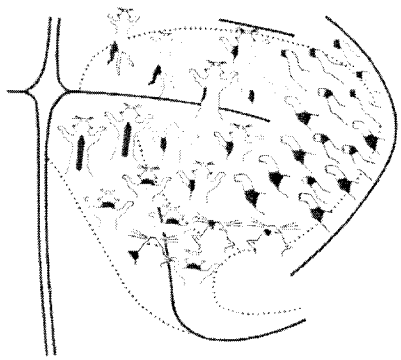

Figure 1.2 Somatotopic organization in the cat motor cortex.

1.3.3 Separation of Multi-Channel Spinal Cord Recordings

Recordings of cortically evoked motor signals from the CST with non-penetrating multi-contact electrodes have been investigated for spatial selectivity [50, 51]. The preliminary data in acute cats showed that the cortically evoked motor signals could be recorded with spatial selectivity from the cervical spinal cord surface. The underlying hypothesis of this approach is that there is a functional organization in the cross-section of the CST of the spinal cord white matter and that the fibers carrying signals from different parts of the motor cortex are grouped to a certain extent. The selectivity obtained with the epidural or intradural recordings during stimulation of cortical points that were at least 1 mm apart suggested the presence of this organization. The average spatial selectivity, based on Euclidean distance [52], was 26 ± 10%, 17 ± 7%, and 15 ± 6% when two, three, and four neural channels were included in the analysis [50]. Although the spatial selectivity level, i.e., the channel separation obtained in these preliminary tests was useful, it could benefit from further improvements for this method to be used as a multi-channel neural interface. Such a neural interface that uses the CST activity proximal to the point of injury may serve as a SCCI for individuals with high-level SCI. The signals generated through this interface can then be used to substitute for the lost voluntary motor control.

1.3.4 Objectives

The main objective of this study is to explore the feasibility of extracting the voluntary motor signals from the LCST and RST in the cervical spinal cord. The long-term goal is the realization of SCCI, which has a long way to go. Thus basic neuroscience and neural signal processing aspects motivate this study.

The aim of the neuroscience aspect is to investigate the functional organization of the motor tracts in the dorsolateral funiculus of the cervical spinal cord using electrical stimulation of the descending tracts with microelectrodes. Evoked electromyogram (EMG) activities recorded from forelimb muscles and observed individual muscle response and limb movements were studied. The species used in this research was the cat. The neuroscience aspect is not only the main body of this dissertation but also the fundamental building block of the future research that could lead to the ultimate realization of SCCI.

In the neural signal processing aspect, the goal is to explore the feasibility and effectiveness of the blind source separation (BSS) technique in improving the separation of spinal cord motor signals. Although direct recording with microelectrode arrays could generate high quality signals, epidural recording of the motor tracts is preferable since it is less invasive and the implantation of the electrodes is much easier. The tissue response of epidural recording would be much less compared with direct recording technique. The improvement of the channel separation (or spatial selectivity) of multi-channel spinal cord recording and the increase of the information rate of neural interface will benefit the SCCI substantially.

1.4 Impact of this Dissertation

The presence of an organization within the dorsolateral funiculus by electrically stimulating the tract fibers at the cervical level of the spinal cord is investigated in this dissertation. The evoked muscle activities are used to determine the degree of the organization, in contrast to the axon tracing studies where the organization in the motor cortex was taken as reference. This study is an attempt to gain new insights into a long-

standing question by using a methodology that was not employed to address this problem before.

Although the BSS technique has been widely applied in biomedical signal processing, its feasibility and performance in the separation of the multi-channel neural recordings from the spinal cord surface has not been studied before. The successful separation of the neural channels could lead to a substantial increase in the information rate of such neural interface. Such a question has been raised: "Can PCA, the more well-established and easier method, do the same job?" This study answers the question and investigates the application of BSS technique in spinal cord neural recordings for the first time.

1.5 Organization of this Dissertation

This dissertation contains seven chapters. The introduction of spinal cord injury, related research and motivation is represented in the first chapter. Background knowledge, including anatomy and physiology of the spinal cord and descending tracts, and the signal processing technique used in this study, is introduced in the second chapter. For the neuroscience aspect of this study, which is the investigation of functional organization of the descending tracts in the cervical spinal cord, Chapter 3 describes the methods, such as experiment protocol, instrumentation, and data analysis procedure, and Chapter 4 gives the results and discussion. Chapter 5 and Chapter 6 concentrate on the neural signal processing aspect of this study. Chapter 5 describes the exploration of the effectiveness of the BSS method in separation of simulated multi-channel spinal cord recordings. In Chapter 6, the feasibility of increasing the separation of spinal cord motor

signals by eliminating the secondary sources, using FastICA algorithm, is presented. Chapter 7 summarizes the conclusions and future research of this study.

CHAPTER 2

BACKGROUND

2.1 Anatomy and Physiology of Spinal Cord

The nervous system consists of the central nervous system (CNS) and the peripheral nervous system (PNS). The brain and the spinal cord, encased in the skull and the bony vertebral column respectively, constitute the CNS.

The spinal cord is attached to the brain stem and extends from the brain to the lower back. The vertebral column (or spinal column) consists of 33 vertebrae. The spinal cord is divided into 30 specific neurological segments according to the vertebra from which the spinal nerves originate. The spinal segments are grouped into four divisions: cervical (C1-C8), thoracic (T1-T12), lumbar (L1-L5), and sacral (S1-S5) (Figure 2.1 [53]).

The spinal cord is comprised of an inner core of gray matter and the surrounding white matter. Gray matter consists of cell bodies and dendrites, whereas the white matter is made up of axon bundles. The spinal cord sends and receives information, which controls sensations, movement, and autonomic functions, from the entire body and the brain [54]. The axon bundles of the spinal cord travel through the body in two pathways: ascending pathway and descending pathway (Figure 2.2 [55]). The ascending pathway carries messages about sensation from the skin and other body parts and organs to the

brain. The descending pathway, which controls movement, carries information from the brain to the motor neurons in the spinal cord and then to the final destination in the body. The somatic motor neurons in the ventral horn of the spinal cord that innervate the somatic musculature are called the "lower motor neurons." Accordingly the motor neurons of the brain that supply input to the spinal cord are called "upper motor neurons."

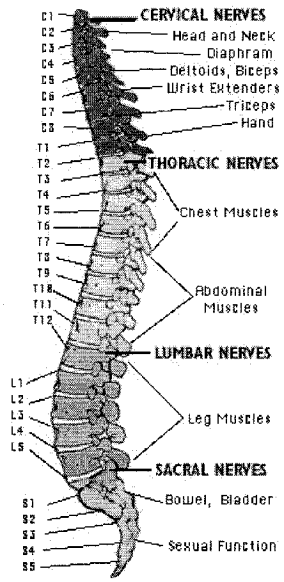

Figure 2.1 Segmental organization of the spinal cord.

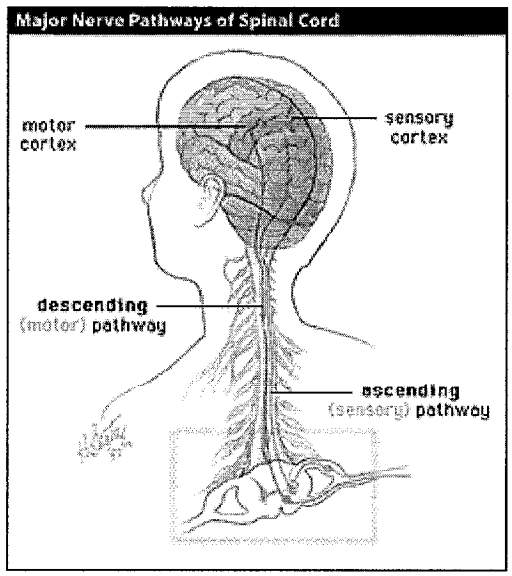

Figure 2.2 The two pathways of the spinal cord.

The spinal cord communicates with the body via the spinal nerves, which consist of both sensory and motor axons. The spinal nerves exit and enter at each vertebral level and communicate with specific areas of the body. Two spinal enlargements contain the greatest amount of gray matter: the cervical and the lumbar enlargements. The nerves that arise from the cervical enlargement supply the upper extremities, while the nerves from the lumbar enlargement supply the lower extremities.

2.2 Descending Tracts

The axon fibers that descend in the white matter of the spinal cord from different supraspinal centers are segregated into different descending tracts (Figure 2.3 [56]). Among these descending tracts, the corticospinal tract (CST) and the rubrospinal tract (RST) constitute the lateral pathway of the motor control, which is under direct cortical control and involved in the voluntary movement of the distal musculature [35].

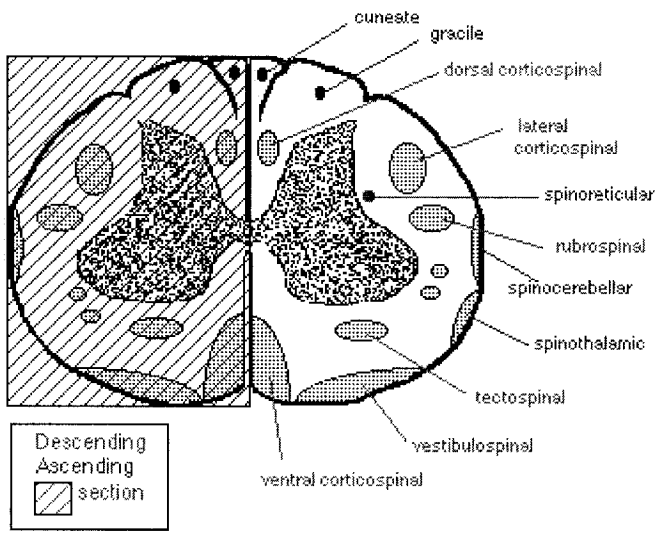

Figure 2.3 Cross section of the spinal cord showing descending and ascending tracts.

2.2.1 Corticospinal Tract (CST)

The corticospinal tract (CST) originates from the motor cortex (areas 4 and 6) in the precentral gyrus of the brain. The fibers of CST pass downwards into the internal capsule and then run in the cerebral peduncles on the anterior aspect of the midbrain. In the pons the fibers are scattered, but they regroup to form the pyramids on the anterior aspect of the medulla. The majority of the motor fibers from the motor cortex decussates in the lower medulla and descends as the lateral corticospinal tract (LCST), which is the principal motor pathway in humans for the control of distal musculature. A few fibers do not decussate but instead descend in the ipsilateral ventral columns as the ventral (or anterior) corticospinal tract (VCST). The VCST is mostly involved in the control of the neck, shoulder, and upper trunk muscles. Figure 2.4 [57] shows the entire route of the CST.

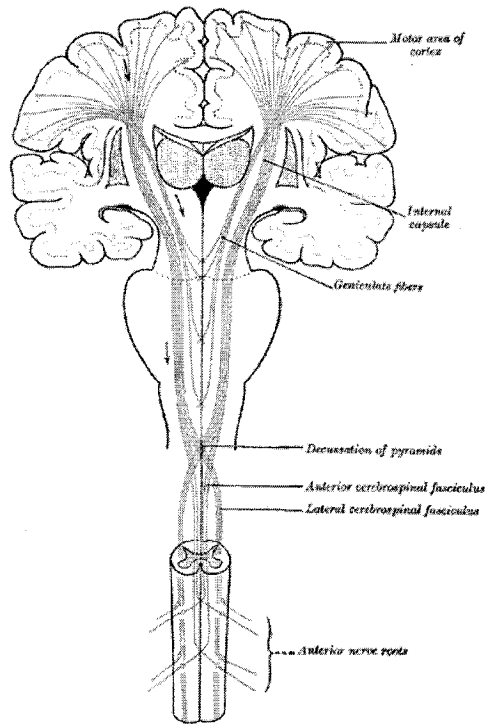

Figure 2.4 Diagram of the corticospinal tract.

Most corticospinal neurons ("upper motor neurons") synapse with the interneurons in the gray matter of the spinal cord. The interneurons then connect with the "lower motor neurons" that innervate the muscles at the motor endplate. The motor impulses from the motor cortex are thus conveyed by the CST contralaterally to control the voluntary movement of the distal musculature.

2.2.2 Rubrospinal Tract (RST)

The rubrospinal tract (RST) originates in the red nucleus in the midbrain. It decussated in the pons and joins the LCST in the lateral column of the spinal cord. Corticospinal and rubrospinal systems are closely interrelated and tend to share common interneurons and propriospinal neurons at the spinal cord level [58-61].

From the cross-section view of the spinal cord (Figure 2.3), the LCST and the RST occupy the dorsolateral funiculus of the white matter. They make up a large portion of the spinal cord white matter at the cervical level. This fact allows the recording of their activities from the spinal cord surface.

2.3 Blind Source Separation (BSS)

In many cases of signal processing applications, the signal received by a sensor is the sum of elementary contributions from various sources. In general, the sources and their mixing proportions at the sensors are not known. The problem of extracting the sources from the sensor measurements without any prior knowledge on the sources (except the assumption of independence) is called blind source separation (BSS) [62]. The underlying principle in solving this problem is called independent component analysis (ICA) [63].

2.4 Independent Component Analysis (ICA)

Independent component analysis (ICA) is a statistical technique for transformation of multidimensional random vectors into components that are statistically as independent from each other as possible. ICA has received much attention in biomedical signal processing in recent years [64-69].

2.4.1 Definition of ICA

The concept of ICA is formulated as the search for a linear transformation that minimizes the mutual information of the estimated components [63]. To define ICA [63, 70], a statistical model in vector-matrix notation is used:

$$\boldsymbol{x} = \boldsymbol{A}\boldsymbol{s}, \tag{2.1}$$

where $\boldsymbol{x}$ is the signal measured at the output of the sensors, $\boldsymbol{s}$ is the unknown signal emitted by the sources. $\boldsymbol{A}$ is the unknown mixing matrix. This model can also be expressed as:

$$\boldsymbol{x} = \sum_{i=1}^{n} \boldsymbol{a}_i \boldsymbol{s}_i . \tag{2.2}$$

This linear model is called ICA model [71], indicating that the observed sensor signal is a linear mixture of the source signals, which stands true for general signal processing problems. A noise term can be added to this model in many applications.

After estimating the mixing matrix $\boldsymbol{A}$ by ICA algorithms, the inverse of $\boldsymbol{A}$ can be computed and denoted as de-mixing matrix $\boldsymbol{W}$. Therefore, the source signals (independent components) can be obtained by:

$$\boldsymbol{s} = \boldsymbol{W}\boldsymbol{x}, \tag{2.3}$$

where $\boldsymbol{W} = \boldsymbol{A}^{-1}$. Thus finding the mixing matrix $\boldsymbol{A}$ is the goal of the algorithms performing ICA.

2.4.2 Assumptions and Ambiguities of ICA

The solution of the ICA problem is based on two very important assumptions:

- The components of $\boldsymbol{s}$ are statistically *independent*.
- The independent components must have *nongaussian* distributions.

The BSS technique is also called "waveform preserved blind estimation of multiple independent sources" [72]. Since both $\boldsymbol{s}$ and $\boldsymbol{A}$ are unknown in the equation (2.1), the following ambiguities hold for the ICA model:

- The variances (energies) of the independent components cannot be determined. Generally it is assumed that each component has unit variance ($\boldsymbol{E}\{s_i^2\}=1$) since $\boldsymbol{s}$ is a random variable. However, the sign is still undeterminable.
- The order of the arrangement of the independent components at the output of the ICA algorithm cannot be determined.

Fortunately, especially for multi-sensor biomedical measurements, the most important information about the source signals is contained in the waveform. Thus, the BSS method is a powerful tool in dealing with biomedical signals.

2.4.3 Comparison between ICA and Principal Component Analysis (PCA)

Principal component analysis (PCA) is a classical statistical method which has been widely used in data analysis and compression [62]. Table 2.1 shows the comparison between ICA and PCA.

Table 2.1 Comparison between ICA and PCA.

ICA	PCA
Imposes statistical independence on all the individual components of the output vector	Imposes independence only to the 2nd order statistics
No orthogonality constraint	Constrains the direction of vectors to be orthogonal
Ensures output pairs are *independent*	Ensures output pairs are *uncorrelated*
Effective method for extraction of independent features	Effective method for data compression

2.4.4 ICA Algorithms

To solve the problem of ICA, Jutten and Herault first developed a feedback fully recurrent neural network and an unsupervised learning algorithm in 1991 [70, 73, 74]. The main characteristic of this algorithm is an independence test using higher-order statistical moments with non-linear activation functions. This algorithm is based on an adaptive computation of feedback neural network coefficients using a gradient method. It was shown that this algorithm worked very efficiently with electroneurogram (ENG) signals contaminated by EMG activity [69].

As a further improvement and extension of Jutten and Herault's method, Cichocki and Unbehauen proposed two unsupervised, self-normalizing, adaptive learning algorithms for feed-forward and feedback neural network models respectively [72]. The algorithms are robust and work efficiently even for badly scaled and ill-conditioned problems [75].

In 1995, Bell and Sejnowski proposed a simple neural network algorithm, InfoMax, for carrying out ICA [76]. Since then, many investigators have explored new applications of ICA to biomedical signal processing, including electrocardiogram (ECG)

[65], electroencephalogram (EEG) [66], event-related potentials (ERPs) [67], and functional magnetic resonance imaging (fMRI) [68].

2.4.5 FastICA Algorithm

In 1999, Hyvärinen first proposed a non-adaptive algorithm called fixed-point FastICA algorithm [77]. Although the FastICA algorithm is non-adaptive, it has most of the advantages of neural algorithms; i.e., it is parallel, distributed, computationally simple, and requires little memory space.

FastICA algorithm and the underlying contrast functions have a number of advantages over the existing ICA algorithms:

- In contrast to the ICA algorithms based on gradient methods, where the convergence is linear, the convergence of the FastICA algorithm is cubic or at least quadratic. Extensive simulations and experiments on real data have achieved very fast convergence [78].
- There are no step size parameters to choose. This property is in contrast to the ordinary gradient-based ICA algorithms, making the FastICA algorithm easy to use.
- In contrast to many ICA algorithms, where the nonlinearity $\boldsymbol{g}$ must be chosen according to some available estimate of the probability distribution function, the FastICA algorithm can directly find independent components of practically any non-gaussian distribution using any nonlinearity $\boldsymbol{g}$. Furthermore, the performance of the neural network can be optimized by selecting an appropriate nonlinearity $\boldsymbol{g}$.

- The independent components can be estimated one by one at the output, especially useful in the applications where only some of the independent components are needed.

CHAPTER 3

METHODS

3.1 Experimental Set-up

3.1.1 Surgery Procedure

Seven adult male cats (~ 3 kg) were used in this study. Anesthesia was initiated with xylazine (2 mg/kg, SC) and ketamine hydrochloride (15 mg/kg, IM) and maintained with 1% alpha-chloralose (20 mg/kg, IV) with subsequent doses when needed. Each cat was intubated and mechanically ventilated to keep the end tidal CO_2 between 3-5%. The femoral vein and artery were catheterized for administration of drugs and monitoring the arterial blood pressure. Rectal temperature was kept between 37-38^{o}C using a heated-top surgical table. Ten to fourteen forelimb muscles shown in Figure 3.1 [79, 80] were implanted with multi-strand, stainless steel, Teflon-coated wires under direct vision with incisions on the medial and lateral sides of the forelimbs for recordings of the muscle activities. Each surgically implanted bipolar EMG wire electrode pair was tested by applying a stimulus and subsequently observing the muscle contraction. The muscles of interest were separated from the neighboring muscles around the belly of the muscle, where the wire electrodes were implanted, and mineral oil was applied to minimize the EMG crosstalk. The selected forelimb muscles were divided into six groups according to their physiological functions (Table 3.1).

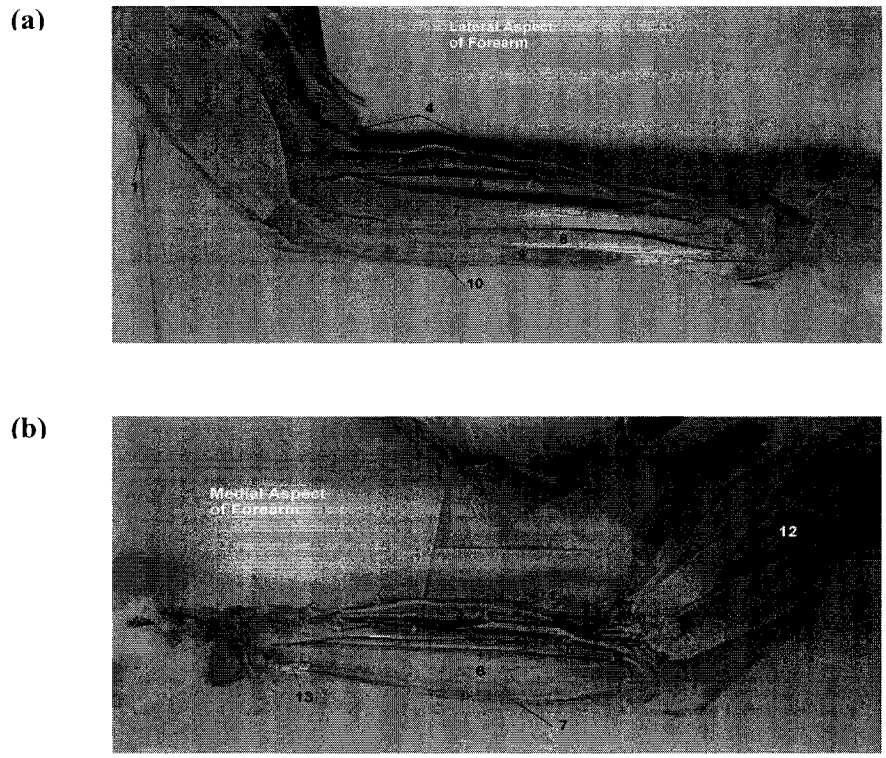

Figure 3.1 Pictures of cat forelimb muscles (refer to Table 3.1 for muscle abbreviations).
(a) Lateral aspect of forearm: 1. LoTriC; 2. LaTriC; 3. Bra; 4. BraR; 5. ECRL; 6. ECRB; 7. EDC; 8. EDL; 9. ECU; 10. FCU.
(b) Medial aspect of forearm: 1. BraR; 2. ECRL; 3. ECRB; 5. FCR; 6. PL; 7. FCU; 8. Cdel; 9. Bi; 11. LoTriC.

A C4-C8 dorsal laminectomy was made to expose the cervical spinal cord. The animal was placed in a stereotaxic frame, and the spinal column was stabilized with a clamp at the spinous process of the first thoracic vertebra. The dura mater was glued using octyl cyanoacrylate adhesive (Nexaband, #500280, World Precision Instruments) to the cut edges of the vertebrae around the periphery of the laminectomy at selected points to stabilize the cord and eliminate movements due to respiration and muscle activation. The laminectomy site was filled with normal saline. The temperature of the saline pool

was kept between 38-40°C by circulating warm water through a small metal pipe placed in this saline pool.

Table 3.1 Six groups of forelimb muscles and their abbreviations.

	Muscle Name	Abbreviation
Elbow Extensor	Long head of triceps	LoTriC
	Lateral head of triceps	LaTriC
Elbow Flexor	Brachialis	Bra
	Brachioradialis	BraR
	Biceps	Bi
Wrist Extensor	Extensor carpi ulnaris	ECU
	Extensor carpi radialis brevis	ECRB
	Extensor carpi radialis longus	ECRL
Wrist Flexor	Flexor carpi ulnaris	FCU
	Flexor carpi radialis	FCR
	Palmaris longus	PL
Digit Extensor	Extensor digitorium communis	EDC
	Extensor digitorium lateralis	EDL
Shoulder Muscle	Clavodeltoid	Cdel

3.1.2 Instrumentation

3.1.2.1 Stimulation Electrode

A single-shank Michigan acute probe (fabricated by the Center for Neural Communication Technology (CNCT) at University of Michigan) with silicon substrate was used as the stimulation electrode (Figure 3.2). The shank, which is the region of the probe inserted into the tissue, contains 16 iridium contacts. The model used is "3mm50",

which means that the shank length is 3 mm, and the spacing between the contacts is 50 μm.

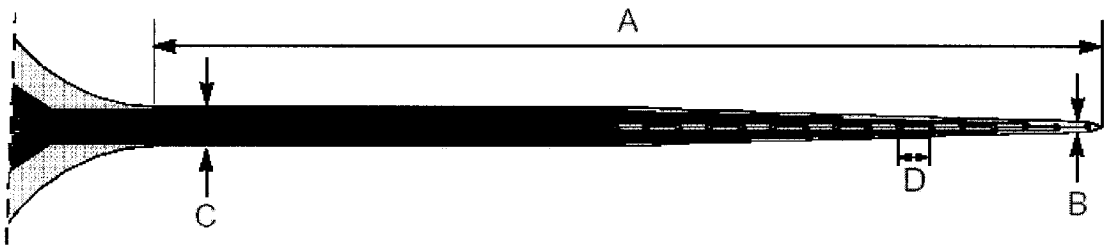

ACUTE NAME	CHRONIC NAME	NUMBER OF SITES	SHANK LENGTH (A)	SHANK WIDTH (B → C)	SITE SPACING (D)	SITE AREA
3mm50	3mm50chron	16	3mm	33 → 123 µm	50µm	177µm^2

Figure 3.2 Single shank Michigan probe and its parameters.

Compared with the Utah Array (UA, Bionic Inc., Utah) and Huntington iridium electrodes (Huntington Medical Research Institute, California), which have quite large tip areas (about 1500~2000 μm^2), the contact area of Michigan probe is only 177 μm^2 (contact diameter: 15 μm). This configuration allows fine stimulation of the fibers in the spinal cord white matter. The Michigan probe has laminar geometry with the thickness being only 15 μm. The tissue it replaces is comparable to that of the Huntington wires and much smaller than that of UAs.

The PC board and the probe tip are shown in Figure 3.3. Iridium activation ("cyclic voltammetry" [81]) was done for the Michigan electrodes used in the experiments. Since the activated iridium oxide is porous and can assume several oxidation states, the charge capacity of the stimulation contacts is increased. Comparison of the electrical characteristics between iridium oxide and titanium nitride indicated that

iridium oxide had lower impedance, higher charge storage capacity, and less power consumption than titanium nitride [82], which make it an attractive material for electrical stimulation of neural tissue. Another important fact is that iridium stores charge by reversible reactions, which is a key consideration for biocompatibility [83].

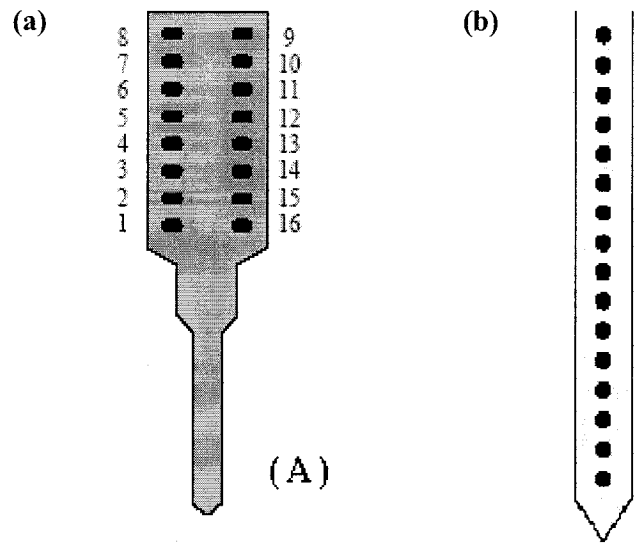

Figure 3.3 (a) PC board.
(b) Probe tip of the single shank 16-channel Michigan electrode.

3.1.2.2 Stimulation and Data Acquisition Software Developed Using LabVIEW

The stimulation and data acquisition software used in the animal experiments was developed using LabVIEW (National Instruments), a graphical programming language used primarily in data acquisition and instrumentation control. The developed software has the following features (see Appendix A for the front panel of the software):

- The analog acquisition from the input channels is triggered by the analog output of the stimulus pulse train. This design not only spares the need of an external trigger but also allows the simultaneous occurrence of the stimulation and the acquisition procedures.

- The user-friendly interface allows the user to define the parameters of the stimulus pulse train and data acquisition. The stimulus waveform will display on the panel for the user to confirm its correctness. The acquired data will be saved as the type that the user defines (text-only (.txt) file in this study).
- Real-time display of the acquired 16-channel signals on the screen. The display modes can be switched between "real-time" and "averaged" versions of the acquired signals.
- The experimental information—such as the parameters used for the stimulation and acquisition, the name and path of the saved data files, and notes and comments—will be saved to a header file. This helps the user to keep a good record of the experiment.

3.1.2.3 Stimulus Waveform

The stimulus waveform used in this study was a charge-balanced, cathodic first biphasic current pulse (Figure 3.4), which is recommended for neural prostheses for the purpose of avoiding tissue damage. Since the cathodic pulse is responsible for the excitation, it was designed having an amplitude of four times that of the anodic pulse. The delay between the two phases was set as 0.2 ms, not only to ensure the effect of the anodic phase which is to turn off the regenerative depolarization process initiated by the cathodic phase, but also to minimize the threshold increase effect of the biphasic waveform compared with monophasic stimulus current.

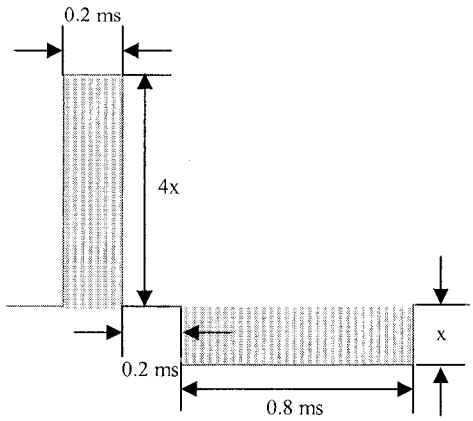

Figure 3.4 Stimulus waveform showing a charge-balanced cathodic first biphasic current pulse.

The parameters of the stimulus pulse train are listed as following:

- Pulse frequency: 330 Hz;
- Duration of the cathodic phase: 0.2 ms;
- Duration of the anodic phase: 0.8 ms;
- Delay between the cathodic and the anodic phases: 0.2 ms;
- Amplitude of the cathodic phase is four times that of the anodic phase;
- Pulse train frequency: 1 Hz;
- Pulse train duration: 20 ms;
- Number of pulse trains for the stimulation of each contact: 16.

3.1.3 Stimulation and Data Acquisition Protocol

Effort was made to minimize the disturbance to the spinal cord during the stimulation procedure. A small medio-lateral cut was made with a 25-gauge needle in the dura mater of the spinal segmental border C5/C6 or C6/C7. A silicon substrate single shank Michigan electrode with activated iridium-oxide contacts was inserted in the cord

vertically at the border of the dorsal entry zone (Zone of Lissauer) and advanced twice down to scan a depth of 0.25-2.55 mm from the surface of the pia mater. A piezoelectric crystal was attached to the electrode holder and driven by a Grass stimulator to vibrate the tip of the electrode at several hundred cycles per second and thus reduce the dimpling effect as the electrode was being inserted into the pia. Electrode contacts were connected, one at a time sequentially through a switch box, to the current stimulator controlled by the computer. A stimulus train of 330 Hz was applied for a duration of 20 ms to each contact individually to generate muscle activity. The resulting muscle activities were acquired into a computer at a sampling rate of 10,000 Hz using a 16-channel neural amplifier (Bionic Inc., Utah, gain = 5,000 or 25,000, BW = 250-7,500 Hz), a data acquisition software (LabVIEW), and an acquisition board (PCI 6023E, National Instruments).

The smallest activation threshold was searched by moving the forelimb in various directions, and then the activity was acquired into the computer at that position. The stimulation and acquisition were done for every other contact of the microelectrode. Then the stimulation electrode was lifted from its last position above the cord and moved 400 μm laterally for another penetration and the stimulation procedure was repeated.

A cross-sectional area of about 2.3 mm by 1.6 mm was scanned in each segmental border (except in one animal, four penetrations only). Figure 3.5 shows the area scanned in the dorsolateral funiculus of C5/C6 segmental border. The drawing was made from a C5/C6 spinal cord histology slide (Figure 3.6) from one of the experimental animals by tracing the edges on the computer. The area in the box was used as the background for plotting the results, where the EMG responses were superimposed on the two

dimensional stimulation points shown on the spinal cord cross-section figure. The horizontal spacing between penetrations was 400 μm and the vertical separation between the stimulation points was 100 μm (every other contact was stimulated and the spacing between contacts was 50 μm). The zero reference point was at the dorsal entry point on the pia surface for all penetrations. The first stimulation point in each penetration was 0.25 mm below the surface and the last one was 2.55 mm deep.

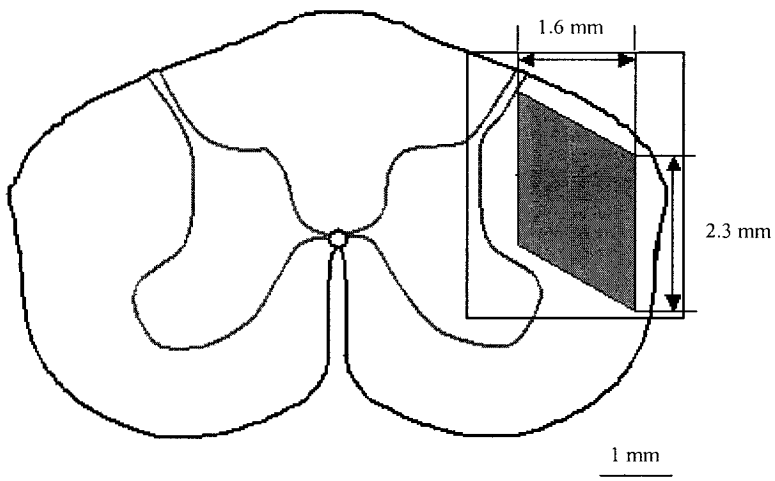

Figure 3.5 Diagram of the cross-section of C5/C6 segmental border showing the scanned area.

At the end of the experiment the spinal cord was removed and fixed in 10% formalin for histology. A histology slice taken from the C5/C6 segmental border is shown in Figure 3.6, where the cleft left by the microelectrode is clearly visible.

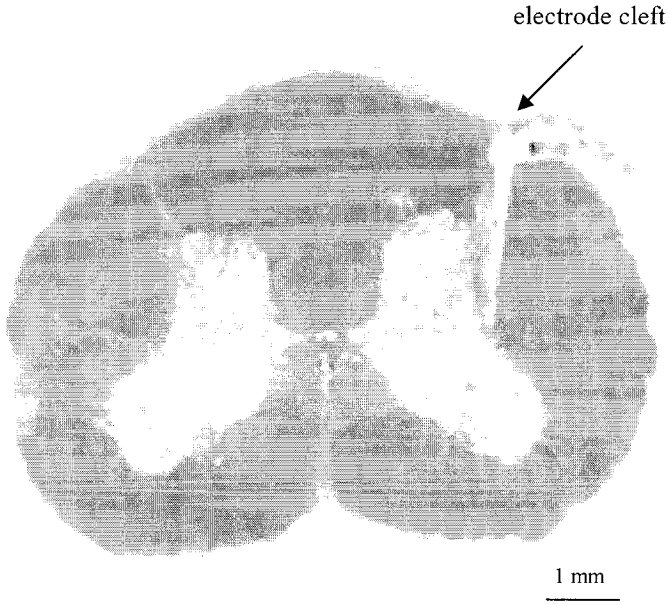

Figure 3.6 Histology picture of a slice taken at C5/C6 segmental border showing the electrode cleft.

3.2 Data Analysis

3.2.1 Data Analysis of EMG Response

EMG signals were first FIR low-pass filtered using 50^{th} order Hamming window with the cut-off frequency set as 1,500 Hz. Then the signals were rectified and integrated within the first 40 ms time window measured from the onset of the first pulse in the stimulus train. Individual muscle responses were plotted on a computer screen one at a time and the arrival and ending time instances of the EMG volleys were marked manually with a mouse click. Figure 3.7 shows how the starting and ending points of the EMG activity were marked. The MATLAB code then rectified and integrated the signal between these two points to find the EMG signal strength. The stimulus artifacts were removed by linear interpolation in cases where the activity was intermingled with artifacts. The EMG signal strength was calculated for each one of the 16 trains applied at

a rate of 1 Hz and the maximum signal strength was taken as the response of that muscle to the stimulation of the point in the spinal cord. The flowchart of the EMG response analysis is shown in Appendix B.

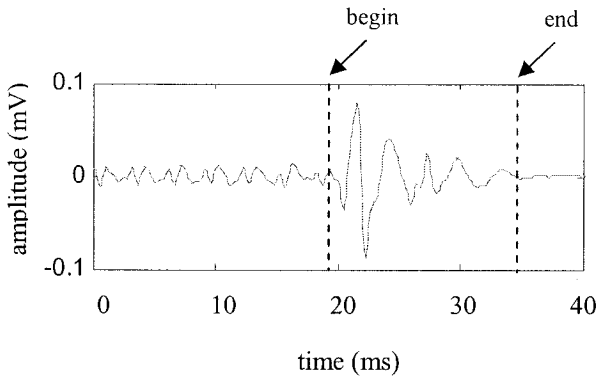

Figure 3.7 The starting and ending points of the activity marked manually to calculate the EMG strength.

3.2.2 Two Normalization Procedures

All the EMG responses underwent two normalization procedures:

- First, all the EMG responses from a given muscle were normalized to the maximum response recorded from that muscle in the same experiment. This was done to eliminate the EMG signal variations across the muscles due to the variation in the recording strengths of the wire electrodes.
- A second normalization was done for each stimulation point in the spinal cord with the maximum of the EMG signals recorded from all the muscles. This second step made the responses comparable for different stimulus strengths used at different points in the spinal cord.

Both of the normalizations described above applied max operation which is better than mean operation. The max operation in the first normalization could detect the

maximal muscle activity evoked at certain point in the cord while the mean operation would tend to average that max EMG value out. The caveat is that the muscle may never be maximally activated anywhere in the spinal cord. But this is a smaller risk than the assumed error that will be made with the mean operation.

The second normalization was done to reduce the effect of stimulation threshold. The stimulus was varied during experiment to get a similar level of activation for all points. However, the activation level was changing. This normalization will help reduce this variability.

The first normalization that minimizes the effect of EMG wire electrodes has to be done first, otherwise some muscles which have good EMG electrodes will dominate all the plots, and it will look as though only these muscles are active.

3.2.3 Choice of Activation Threshold for Analysis

To choose the activation threshold for analysis, the volume of activation related to the current strength needs to be considered. A stimulation pulse of 30 μA amplitude and 0.2 ms duration strength activates a volume of about 200 μm in radius [84]. Since the separation between the penetrations was 400 μm, 35 μA was set as the activation threshold for data analysis to avoid overlapping of the activation volume between the penetrations while trying to cover the whole funiculus in the horizontal direction. However, there would be some overlap in the vertical direction since the separation between two stimulating contacts was 100 μm.

Below 35 μA, the current strengths were further divided into two ranges, below 20 μA and 20-35 μA, to distinguish the relative low and high stimulation currents.

3.2.4 Data Plotting

A two-dimensional matrix of stimulation points were superimposed on a figure representing the dorsolateral funiculus of the cervical spinal cord (the area in the box of Figure 3.5). A small ellipsoidal (for stimulus 0-20 μA) or a rectangular (20-35 μA) symbol was placed at the points of stimulation. The size of the symbol represented the normalized EMG strengths in percentages. Points of high threshold (>35 μA) were shown as small dots. A separate map was generated for each muscle recorded from. Data from multiple experiments were combined by taking the mean of the EMG strengths for the same muscle and for the same stimulation point in the spinal cord across the animals.

Similar to the EMG mapping, figures were generated for the mean current threshold of all the cats for each and every stimulation point in the scanned area of the spinal cord. The threshold values of larger than 50 μA are regarded as very high thresholds and entered as 50 μA into the averaging process. The mean threshold values between 35 and 50 μA are shown as crosses, indicating high current strength.

CHAPTER 4

RESULTS AND DISCUSSION

4.1 Results

4.1.1 Raw EMG Signals

Multiple forelimb muscles were activated at the threshold and suprathreshold currents. Figure 4.1 shows a typical recording from five representative forelimb muscles following a 20 ms stimulus train at 330 Hz. An elbow extensor (LoTriC), an elbow flexor (Bra), a wrist extensor (ECU), a wrist flexor (FCR), and a digit extensor (EDL) are shown. The stimulation artifacts appear during the stimulus train. The arrival times, durations, and the amplitudes of the activities vary. Some arrive before the end of the stimulus train and some others much later. For those EMG responses that arrived before the end of the stimulus train, each pulse generated a single volley that grew larger at the next pulse and eventually triggered a long duration multiphasic muscle activity (see FCR activity). The twitch strength always increased quickly and became very strong as the current was further increased above the threshold. In some cases there was an interruption in the middle of the multiphasic activity giving the appearance that there were two events. Those activities were excluded in the EMG strength analysis unless they occurred within the 40 ms window from the first pulse.

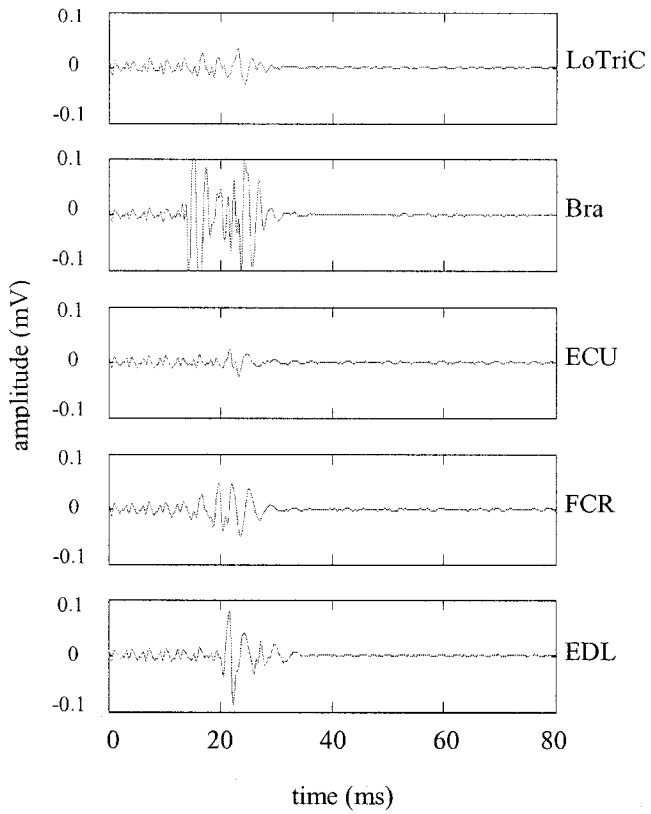

Figure 4.1 Muscle activities recorded from five representative forelimb muscles following a 20 ms stimulation train at 330 Hz.

Muscle responses varied greatly during a trial. The twitch strength varied even between consecutive trains during a 16-second trial (16 trains at 1 Hz) and sometimes diminished by the last train. Some typical activation patterns included cases where there was only one or two muscles increasing and decreasing in strength simultaneously while the activity was minimal or absent in the other muscles. In other cases, the maximum EMG strength switched between two sets of muscles back and forth. Figure 4.2 exemplifies these cases where three muscles change substantially in strengths during a trial. The muscle strengths of long head of triceps (LoTriC) and extensor digitorium communis (EDC) vary in phase and out of phase, while the extensor digitorium lateralis

(EDL) is active in the beginning and disappears later before the end of the trial. In all cases, the maximum activity of each muscle during a 16-train trial was taken as representative muscle activation strength for the stimulation point being tested in the spinal cord.

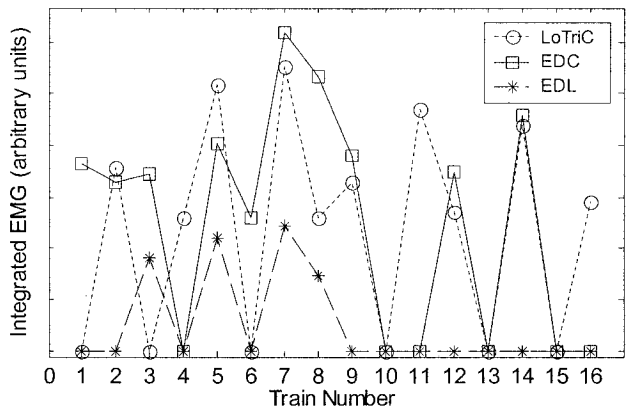

Figure 4.2 EMG strengths of three different muscles during a trial of 16 consecutive trains.

4.1.2 Muscle Activity Maps

Figure 4.3 illustrates the EMG maps for ten forelimb muscles separately on the dorsolateral funiculus at the C5/C6 segmental border of the spinal cord in one cat. Synergistic muscles are grouped together vertically. An ellipsoid indicates a stimulation current of less than 20 μA and a rectangle between 20 and 35 μA. The width of the symbol indicates the strength of the EMG signal. Comparison of these maps reveals that the overlap is extensive. The set of muscles that were active changed gradually, rather than abruptly, as the stimulating contact position moved down in the spinal cord. This in turn caused a large overlap in the muscle maps although the resulting limb function was not the same across these stimulation points. For the same reason, the muscle activity

maps show significant continuity. That is, the EMG strengths varied gradually until a low threshold, large response (large ellipsoid) point was reached. In this animal, there was a region in the middle of the area of stimulation, oriented in the medio-lateral direction, where the EMG responses diminished completely even if a very large stimulus (>35 μA) was applied.

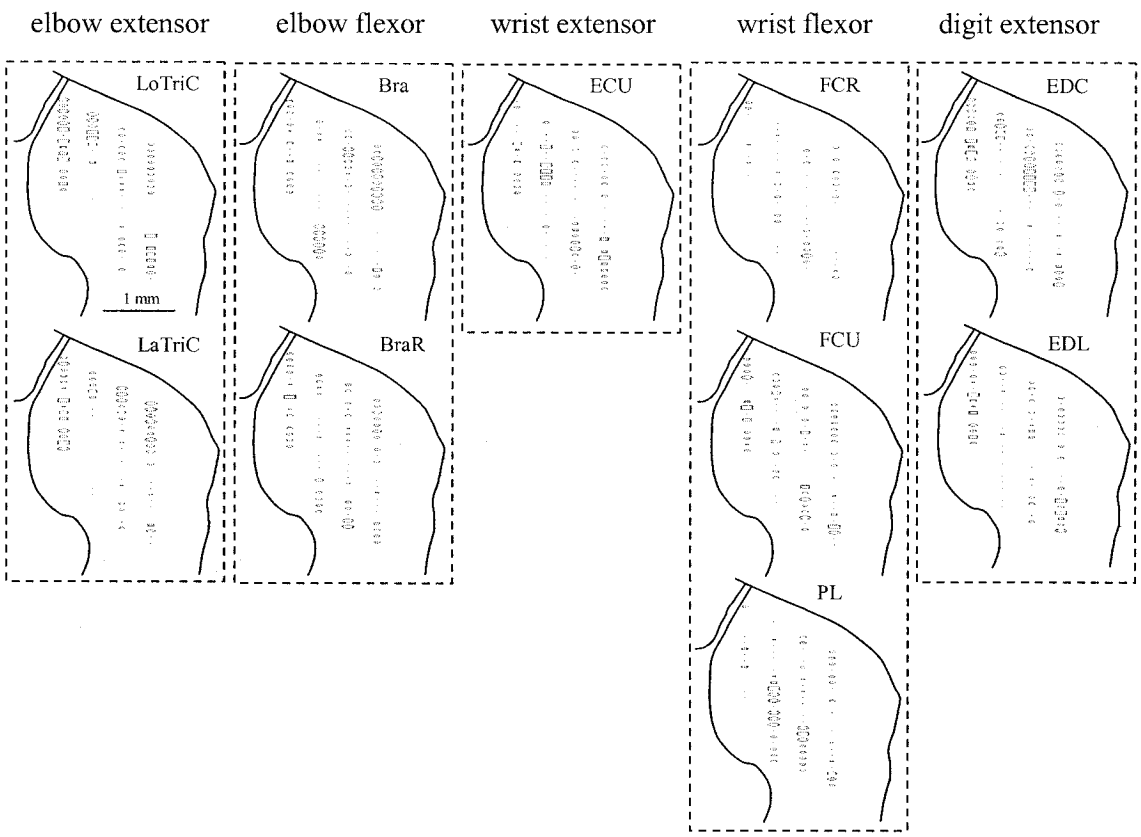

Figure 4.3 The normalized EMG strengths maps for each forelimb muscle separately on the dorsolateral funiculus at the C5/C6 segmental border of the spinal cord in one cat.

The combined maps from all seven cats are shown in Figure 4.4 and 4.5 for C5/C6 and C6/C7 segmental borders respectively, though most of the data were contributed by five animals. The data for ECRL were collected in only two experiments and the data for Cdel were collected in three experiments. Activities of Bi, ECRB, FCU and EDC were recorded in six experiments while the others were collected in all seven experiments. Table 4.1 shows the number of muscles being recorded during each experiment.

Table 4.1 Number of muscles being recorded during each experiment.

Experiment No.	No. of muscles	Muscles
1	12	Except for: ECRL, Cdel
2	11	Except for: EDC, ECRL, Cdel
3	10	Except for: Bi, ECRB, ECRL, Cdel
4	13	Except for: Cdel
5	14	All 14 muscles
6	13	Except for: ECRL
7	12	Except for: FCU, ECRL

The width of the symbol in Figure 4.4 and 4.5 represents the mean of the muscle activities obtained from all the experiments when the stimulus was applied where the symbol is located. A certain degree of organization is found in these combined maps.

In C5/C6 (Figure 4.4), the high threshold area in the middle of the region, similar to Figure 4.3, is still visible for some muscles even after averaging, such as elbow/digit extensors. The elbow flexors (Bra, BraR, and Bi) and digit extensors (EDC and EDL) were the most active muscles as a group. Elbow extensors (LoTriC and LaTriC) were

activated both at dorso-medial and ventro-lateral parts at the funiculus with a clear high-threshold region in the middle. The wrist muscles in general were more readily activated in the ventro-lateral part of the region studied, especially FCR and PL muscles.

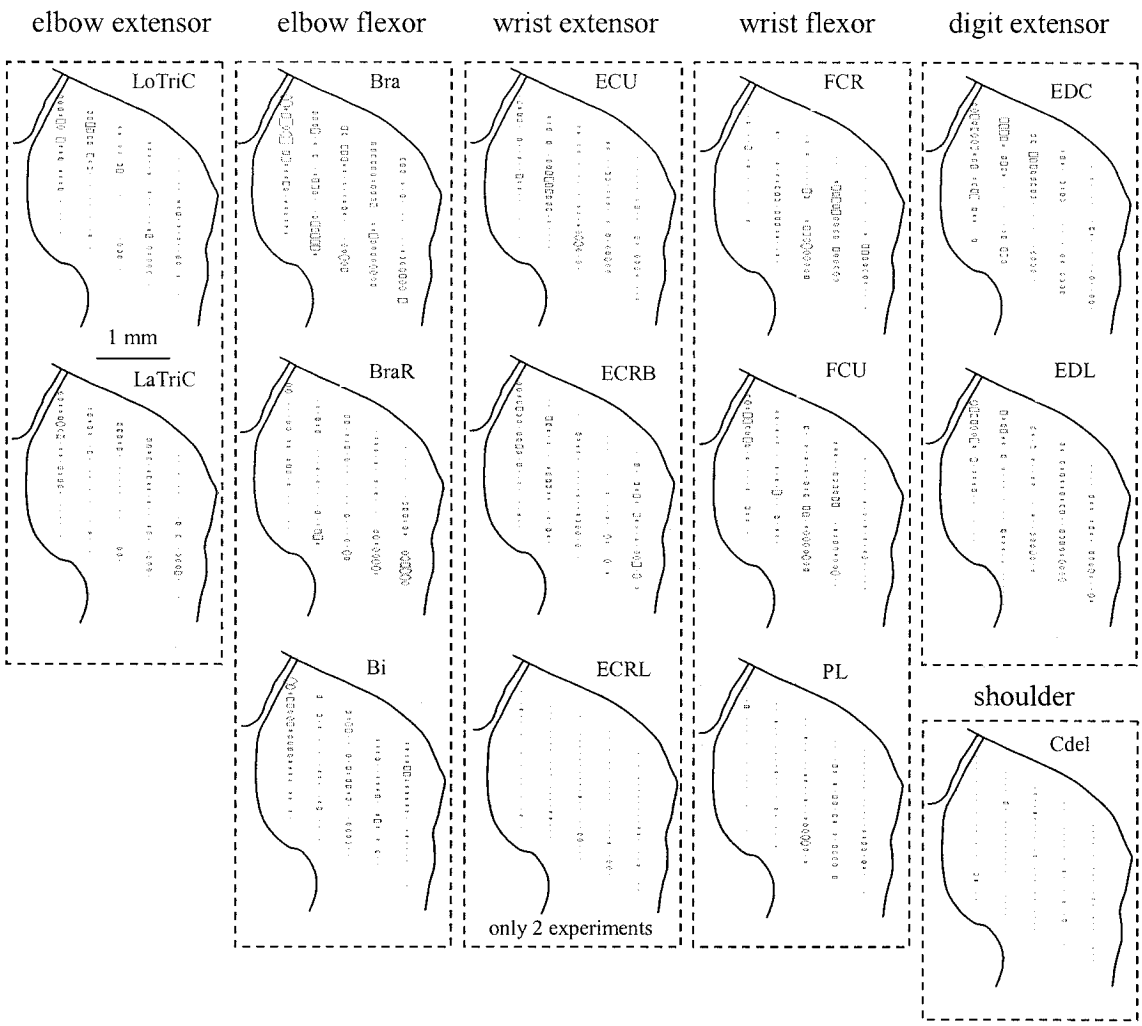

Figure 4.4 The normalized EMG strengths combined from all cats and mapped onto the spinal cord for each muscle individually at C5/C6 segmental border.

In C6/C7 (Figure 4.5), overall the forelimb muscles were activated at a fewer number of stimulation points, which is in agreement with the fact that C6/C7 is more distal in the cervical enlargement than C5/C6. Elbow flexors were the most active as a group and were activated more medially compared to the wrist and digit muscles. The ECRB activity was contained in the ventro-lateral region while FCU and ECU were more frequently stimulated on the medial and dorsal parts of the region, respectively.

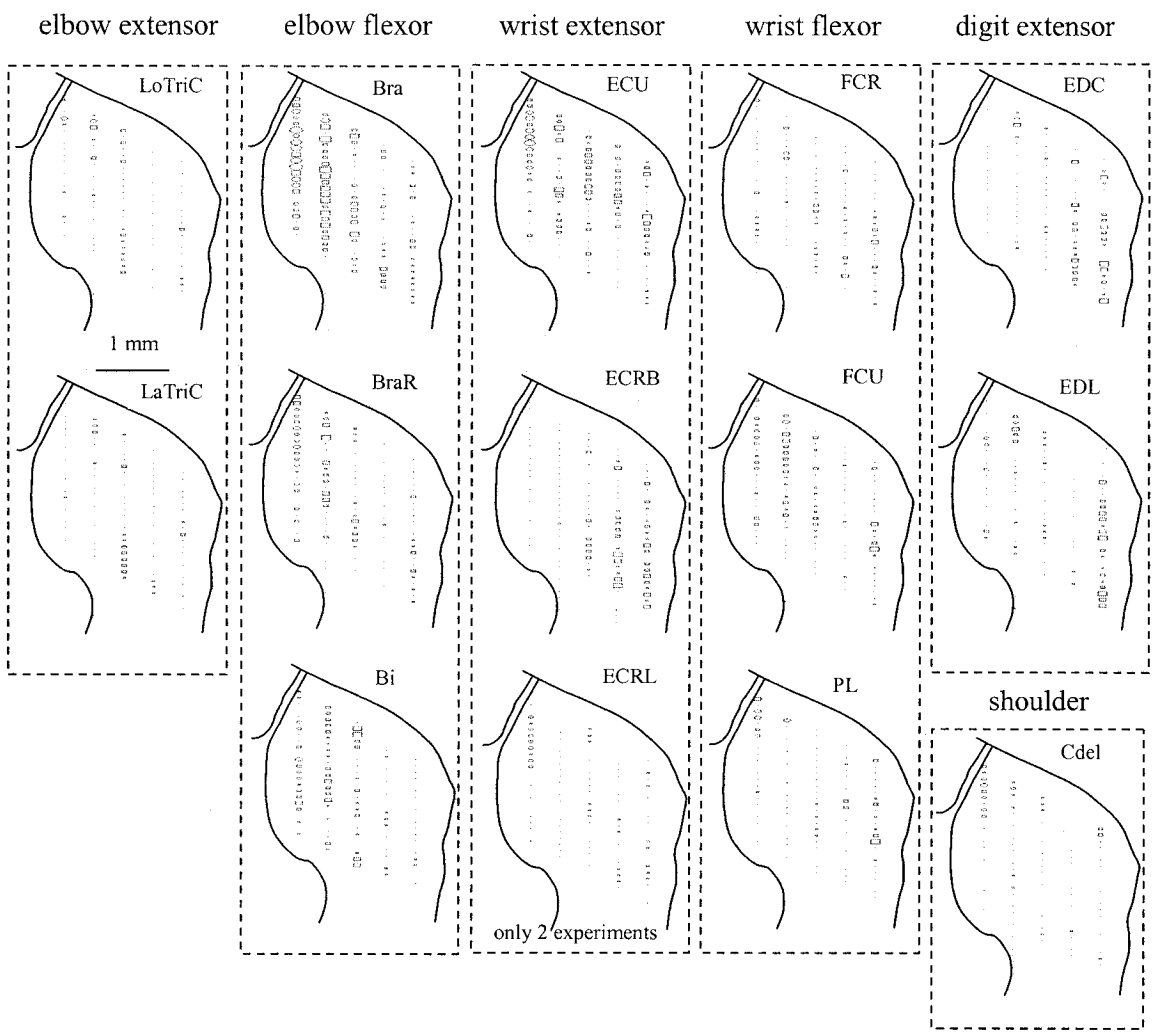

Figure 4.5 The normalized EMG strengths combined from all cats and mapped onto the spinal cord for each muscle individually at C6/C7 segmental border.

4.1.3 Repertoire of Muscle Responses

The following general observations were made during the experiments. The repertoire of the limb movements observed in this study included shoulder jerk, elbow extension/flexion, wrist extension/flexion, digits opening/closing, and single digit movements. Most movements resembled a combination of these main types. Abduction/adduction or supination/pronation of the arm was never observed as distinct limb movements. Other body parts were activated only rarely compared with the total number of observations (1576 times) across all the experiments. Table 4.2 shows the activated muscle movements other than the ipsilateral forelimb muscles.

Table 4.2 Activated muscle movements other than the ipsilateral forelimb muscles.

Experiment No.	Neck	Upper torso (chest and back)	Jaw	Ipsilateral hind legs	Contralateral limb
1	9	6	2	4	2
2	11	9	0	0	0
3	5	14	4	0	16
4	9	8	0	0	2
5	0	3	0	0	0
6	8	18	1	3	3
7	2	4	1	3	1
Total	**44**	**62**	**8**	**10**	**24 (19 hindlimb)**

We occasionally tested if the twitch-like limb movements observed with a short stimulus train could turn into sustained forces with longer trains (>1000 ms). This test was done in five cats for various limb movements. Out of 74 tests, 29 (39.2%) showed sustainable movements, most of which were flexions of forelimb joints.

4.1.4 Activation Thresholds

In this study, we looked for the lowest threshold by passively moving the forelimb in various directions before collecting the data for each stimulation point. This procedure sometimes reduced the threshold, and at other times the effect was not appreciable. However, the type of limb movement observed did not change whether the limb was at a low threshold position or elsewhere. The muscle twitches became much stronger as a low threshold position was approached and thus the stimulus level had to be reduced subsequently. The minimum threshold ever observed was 5 μA (only twice). Threshold levels less than 10 μA were recorded 14 times. The points where current amplitudes even larger than 35 μA did not elicit a twitch were classified as high threshold points (dots on the activation maps).

The average stimulation thresholds are shown in Figure 4.6 and 4.7 for C5/C6 and C6/C7 segmental borders respectively. The size of the rectangle indicates the intensity of the current threshold. The box size that represents a 50 μA stimulus is shown in the upper right corner. The points where the mean threshold was larger than 35 μA are indicated with a cross. If the threshold was larger than 50 μA, it was entered as 50 μA into averaging. The largest thresholds were to be found in the middle of the funiculus, whereas the low threshold points were concentrated at the dorso-medial and ventro-lateral parts of the funiculus, at both segmental borders studied.

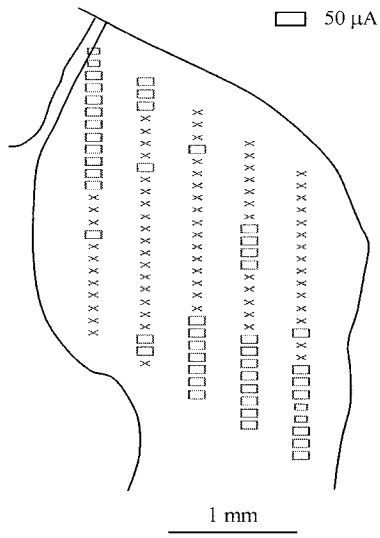

Figure 4.6 The average of stimulation current thresholds mapped on the dorsolateral funiculus of C5/C6 segmental border.

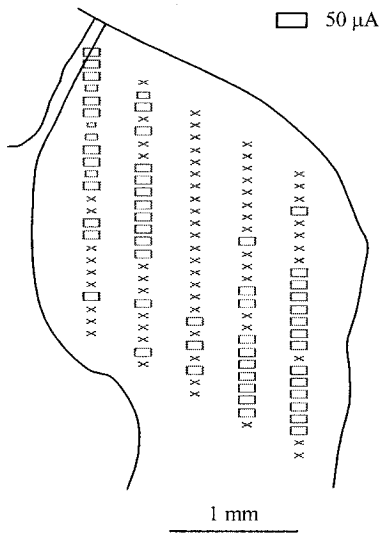

Figure 4.7 The average of stimulation current thresholds mapped on the dorsolateral funiculus of C6/C7 segmental border.

4.2 Discussion

4.2.1 Activation Maps

A degree of functional organization was found in the descending tracts of the dorsolateral funiculus in the cervical segmental borders. The organization in the combined maps (Figures 4.4 and 4.5) is weaker than the maps from individual animals (Figure 4.3). This effect might be due to the fact that the EMG responses were averaged across all cats. Since the organization varied from animal to animal, the averaging process can make the maps less distinctly defined.

The movement patterns did not change abruptly from contact to contact along the electrode. A stimulation pulse of 30 μA amplitude and 0.2 ms duration strength activates a volume of about 200 μm in radius [84]. Although the volumes of activation should be well separated in the horizontal direction as a result of 400 μm between the penetrations, there will be some overlap of the activated volumes in the vertical direction since we stimulated at every 100 μm. This effect in turn can explain some of the fuzziness in the muscle maps.

The organization may also be changing along the cervical cord as the fibers terminate in the gray matter at various segments as they descend. A study of the multiple axon collaterals of a single corticospinal neuron showed divergent distribution to different levels of the spinal cord in the cat [47]. In our study, at many stimulation points in the spinal cord the muscle activities resulted in a functional limb movement, i.e., flexion or extension of a limb segment. However, at many others there was a co-contraction of the flexors and extensors, which is in agreement with the findings of Armstrong et al. during locomotion in cats [85]. This observation suggests that there is

extensive intermingling of the fibers destined to control antagonistic limb functions.

Multiple muscles were activated at each stimulation point even at the threshold stimulus. Unlike the monkey, where a direct cortico-motoneuronal projection exists [41], a direct synaptic connection between the LCST fibers and the alpha motoneurons of the ventral horn reportedly does not exist in the cat [86, 87]. That multiple muscles were activated at each stimulation point was expected since the lateral corticospinal fibers in the cat mainly synapse on the interneurons of the laminae V-VII [49] and not on the alpha motoneurons directly. Stimulation of the interneuronal circuit resulted in activation of multiple muscles generating a net force around the hindlimb in the cat [85]. The variability of movement patterns elicited by pyramidal stimulation in the decerebrate cat was ascribed to the complex spinal interneuronal system [88] and partially due to the varying spread of the stimulus to neighboring structures [87]. The disynaptic pathways of the forelimb control are mediated by two different interneuronal systems, the propriospinal neurons located in layer VII of the C3-C4 segments [89-91] and the interneurons in the forelimb segments [92]. The C3-C4 propriospinal neurons terminate in the cervical enlargement [90] and play an important role in mediating the forelimb control. Despite the abundance of the synaptic activation in the cat, we also observed EMG patterns, although very rarely, where the signal was repeated exactly without variation in pattern or strength in some muscles. This finding in combination with the finding that some of our tracing attempts stained cells in the 9^{th} lamina of the gray matter (unpublished results) suggest that there may be a few descending axons that are directly synapsing on the alpha motoneurons.

It is shown in a study that the pyramidal excitation dominated in motoneurons to flexors of all joints of forelimb [92]. In our study the flexor muscles were activated more frequently than extensors. This result is in agreement with the finding of Armstrong et al. where the flexor muscles of the forelimbs had lower thresholds than extensors during stimulation of the motor cortex in unanesthetized cats at rest [93]. The activation thresholds were lower during walking compared to resting mainly due to the increased responsiveness of spinal cord circuits to descending motor signals during locomotion [85].

The LCST and RST make up a large portion of the dorsolateral funiculus, and the areas they cover in the cross-section of the cervical spinal cord white matter overlap to some extent. This fact might explain the high threshold zone observed in the middle of the dorsolateral funiculus, which is more obvious in the C5/C6 segmental border. The simultaneous stimulation of LCST and RST, or the stimulation of one tract, somewhat spread to the other tract, might result in some cancellation of their effects.

4.2.2 Observed Limb Movements

An interesting finding is that the limb movements were mostly in the form of short twitches, and they were not sustainable even when the stimulation train was made much longer. This observation is in agreement with the cortical mapping studies where the evoked movements were single and non-repetitive [44]. It is in contrast, however, with studies where the intermediate laminae were stimulated at the lumbosacral levels which generated sustained forces for stimulus trains of 200-600 ms [94]. This finding may be explained by the modulation role of the corticospinal tract. LCST is only involved in the control of the fine details of the stereotyped movements or the fine

control of the distal limbs. It was also suggested that the main role of the corticospinal tract is only to control the timing of the limb movements [85]. Alternatively, each group of LCST fibers may be modulating the limb function within a short time window where it is needed during a behavior.

Another interesting observation is that, although the LCST extends down to the level of the sacral spinal segment in the cat [95], hindlimb movements were very rarely observed, only 29 times. The neck, back of the upper torso, and the muscles around the rib cage were more frequently activated (106 times), although still much rare than the forearm muscles, perhaps due to the difference in the activation threshold for various muscles, which is in agreement with some reports on the motor cortex stimulation [44]. We occasionally observed hindlimb movements, especially with longer pulse trains, which tends to lower the activation threshold, while testing if the forces were sustainable.

Similarly, the finding that wrist abduction/adduction and forearm supination/pronation were never observed in this study maybe related to the activation threshold. The movement types that have the lowest threshold dominate and the high threshold ones are obscured.

4.2.3 Concerns about the Signals and Instrumentation

Crosstalk between EMG channels is a possibility. The electrodes were inserted into the belly of the muscles under direct vision following the same procedure in each animal and mineral oil was poured. Although we did not test for crosstalk directly, there existed an episode of data for each muscle where only that muscle was active and no coinciding signal was recorded from the neighboring muscles, indicating that the crosstalk was not significant. Only the muscles that had a unique pattern of activity were

included in the analysis to eliminate the possibility of crosstalk. Furthermore, the max operation applied to the EMG strengths tends to eliminate the low level signals due to crosstalk.

Although the number of afferent fibers in the pyramidal tract is small [86], reflexes might be activated by stimulation of the (ascending) spinocerebellar tract fibers. The EMG activities were analyzed using a short window (40 ms long) following the first pulse. Thus, the possible contribution from the reflex pathways into the recorded EMG activity was minimized.

For the stimulus to go through multi-synaptic pathways of the interneuronal circuitry, at least three or more consecutive pulses are needed [87, 92]. On the other hand, it was in our best interest to keep the stimulus train as short as possible to minimize the stimulus artifact in the recordings. In this study, a pulse train of 20 ms at 330 Hz was chosen to find an optimum point between these trade-offs. In the monkey, the duration of pyramidal stimulation required to produce a response is a characteristic of the muscle and it varies [96].

CHAPTER 5

SEPARATION OF MULTI-CHANNEL RECORDINGS OF CORTICOSPINAL TRACT USING BLIND SOURCE SEPARATION METHOD

5.1 Methods

5.1.1 Data Collection

The data used in this study were from Dr. Mesut Sahin's previous experiments and were reported earlier [50, 51]. Briefly, the motor cortex around the cruciate sulcus was stimulated with the tungsten microelectrodes in four adult cats under ketamine anesthesia. First, pulse train (PW = 0.2 ms, f = 330 Hz, duration = 45 ms) was applied to the motor cortex to evoke muscle twitches in various parts of the contralateral forelimb (occasionally hindlimb) and thereby identify the corresponding areas of the motor cortex. A single pulse (PW = 0.2 ms, I = 800 μA) was then delivered to the motor cortex to evoke a descending motor response in the LCST of the spinal cord. The cortical stimulation points were at least 1 mm apart to assure different groups of fibers were activated within the LCST. The evoked potentials were recorded from the cervical spinal cord surface using one of the three designs (Figure 5.1) of silicone substrate multi-contact electrodes. The signals were acquired into a personal computer at a sampling rate of 80,000 Hz using a National Instruments data acquisition board (PCI-6071E) and the LabVIEW programming tool.

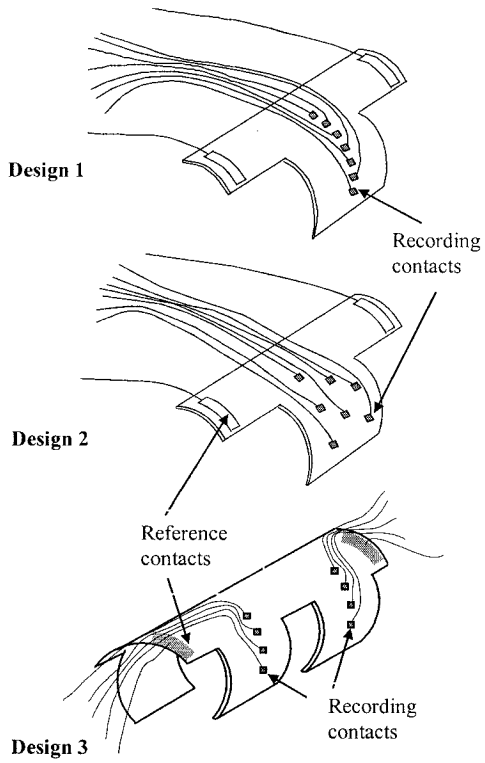

Figure 5.1 Multi-contact electrode designs used for epidural and intradural recordings from the LCST.

Each recording episode had multiple channels (or contacts, 7 contacts for design 1 and 2, and 8 contacts for design 3) and consisted of 256 acquisitions of 10 millisecond neural recordings following the cortical stimulus delivered at a rate of 2 pulses/sec. Multiple acquisitions (n = 256) were stimulus-trigger averaged to extract the motor component in the presence of a large background noise. A single acquisition of a 10 millisecond raw signal with contaminating neural components and background noise is shown in the top panel of Figure 5.2. The bottom panel of Figure 5.2 illustrates a stimulus-trigger averaged version of the signal with the stimulus artifact occurring within the first millisecond. To eliminate the stimulus artifact, the first millisecond of each acquisition was discarded before averaging, and the remaining 9 millisecond neural

signals of the averaged version were padded sequentially to simulate long episodes of spontaneous neural activity.

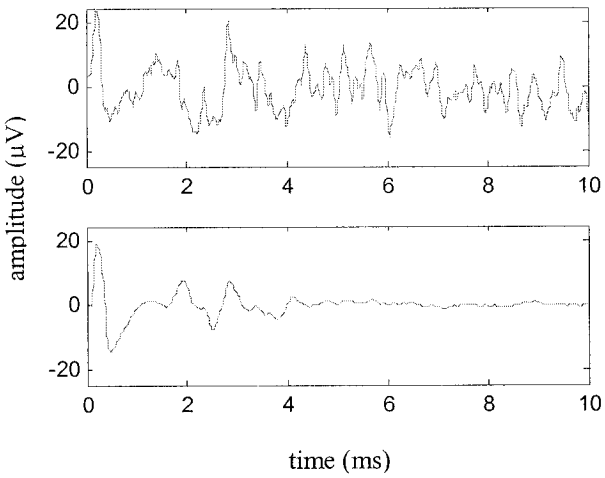

Figure 5.2 Extraction of the motor components from the spinal cord signals using stimulus-trigger averaging (n = 256).

5.1.2 Simulation of Multi-Channel Spinal Cord Recordings

Figure 5.3 shows the signal flow of this study. We analyzed eleven data sets. In each data set, six different neural patterns recorded during stimulation of six different cortical points were selected. These patterns were treated as neural channels in this study since each pattern was presumably generated by a different group of fibers. A typical contact in each episode was selected to represent the neural pattern generated in the spinal cord before it was picked up by the recording electrode. These signals are called source neural patterns (leftmost column in Figure 5.3). Recording of these source patterns with a multi-contact electrode from the spinal cord surface was simulated by multiplying the *unaveraged* version of the source neural patterns with a mixing matrix $\boldsymbol{A}$:

$$\boldsymbol{x}(t) = \boldsymbol{A}\boldsymbol{s}(t), \tag{5.1}$$

where $x(t)$ is the mixed signal, and $s(t)$ is the source signal. The mixing matrix A was chosen as:

$$\mathbf{A} = \begin{bmatrix} \mathbf{1.01} & 1.00 & 1.00 & 1.00 & 1.00 & 1.00 \\ 1.00 & \mathbf{1.01} & 1.00 & 1.00 & 1.00 & 1.00 \\ 1.00 & 1.00 & \mathbf{1.01} & 1.00 & 1.00 & 1.00 \\ 1.00 & 1.00 & 1.00 & \mathbf{1.01} & 1.00 & 1.00 \\ 1.00 & 1.00 & 1.00 & 1.00 & \mathbf{1.01} & 1.00 \\ 1.00 & 1.00 & 1.00 & 1.00 & 1.00 & \mathbf{1.01} \end{bmatrix}. \tag{5.2}$$

The slight variation in the coefficients between the rows simulated the movement of the source in the cord cross-section, hence introducing spatial selectivity. The mixing matrix was selected near singular ($\det(A) = 6.01e^{-10}$, ill-conditioned) to make the initial spatial selectivity very small (1%), based on the Euclidean distance between the vectors [52]. Then, the *unaveraged* version of the simulated multi-contact neural recordings were fed into the BSS algorithm for separation. The output signals of the BSS neural network are called output neural patterns (rightmost column in Figure 5.3). The output patterns were compared with the source patterns using a crosstalk measure to evaluate the performance of the BSS algorithm in separation of multi-channel neural recordings.

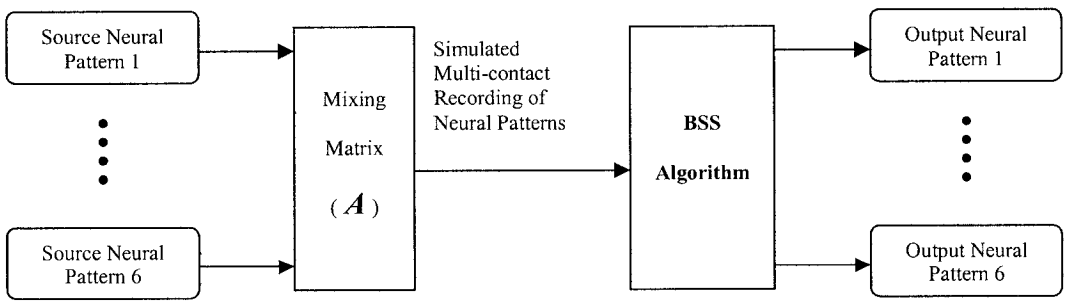

Figure 5.3 The signal flow diagram of this study.

5.1.3 BSS Algorithm

We applied the feed-forward neural network model of the BSS algorithm proposed by Cichocki and Unbehauen [72] to separate the neural channels of the simulated spinal cord recordings.

A single-layer feed-forward neural network with learning capability was used. The iterative learning rule of the BSS neural network coefficients, $\boldsymbol{W}(t)$, based on the gradient method is:

$$\frac{d\boldsymbol{W}(t)}{dt} = \mu(t) \times \left\{\boldsymbol{\Lambda} - \boldsymbol{f}\left[\boldsymbol{y}(t)\right] \times \boldsymbol{g}^{T}\left[\boldsymbol{y}(t)\right]\right\}\boldsymbol{W}(t), \tag{5.3}$$

with $\boldsymbol{W}(0) = \boldsymbol{I}$, and $\boldsymbol{\Lambda} = \boldsymbol{I}$, where $\boldsymbol{I}$ is identity matrix, and $\boldsymbol{y}(t)$ is the output signal. The $\boldsymbol{f}(x)$ and $\boldsymbol{g}(x)$ functions are two different non-linear odd activation functions, which are used to transform the activation level of a unit (neuron) into output signals. In this study, we used $f(x) = x^2 sign(x)$ and $g(x) = \tanh(10x)$. The learning rate $\mu(t) > 0$ is a constant during the first phase ("search" phase of learning), and then it is exponentially decreased to zero in the second phase ("converge" phase of learning).

5.1.4 Definition of Parameters

The definitions of signal-to-noise ratio (SNR), spatial selectivity, and percent crosstalk are introduced as the following.

5.1.4.1 Signal-to-Noise Ratio (SNR)

The SNR was defined as the ratio of the standard deviation of the motor activity ($\boldsymbol{M}$) in the *averaged* signals and that of the background noise ($\boldsymbol{N}$) measured in the *unaveraged* signals while no stimulation was delivered to the cortex:

$$\boldsymbol{SNR} = \frac{\boldsymbol{std}(\boldsymbol{M})}{\boldsymbol{std}(\boldsymbol{N})}. \tag{5.4}$$

The background noise mainly consisted of the sensory activity recorded from the fibers of the dorsal spinocerebellar tract located between the electrode and the corticospinal tract. The noise component was always larger than the motor signals due to the relative proximity of the spinocerebellar tract to the recording electrode.

5.1.4.2 Spatial Selectivity

Chen et al.'s method [52] was used to quantify the spatial selectivity. In our case, the selectivity was artificially determined by the choice of the mixing matrix A. The elements in each row of matrix A formed a six-dimensional measurement vector A_i:

$$A_i = (A_{i1}, A_{i2} \ldots A_{i6}), \; i = 1 \text{ to } 6. \tag{5.5}$$

The measurement vector A_i was then normalized to obtain the feature vector W_i of the corresponding channel:

$$W_i = (W_{i1}, W_{i2} \ldots W_{i6}) = \frac{A_i}{|A_i|}. \tag{5.6}$$

The selectivity index of each channel (S_i) was defined as the average Euclidean distance between the feature vector of that channel and those of the other five channels:

$$S_i = \frac{1}{5}\sum_{j=1}^{6} d_{ij}. \tag{5.7}$$

The Euclidean distance between the feature vectors (d_{ij}) was calculated using the following equation:

$$d_{ij} = \frac{100}{\sqrt{2}}\sqrt{(W_{i1} - W_{j1})^2 + (W_{i2} - W_{j2})^2 + \ldots + (W_{i6} - W_{j6})^2}. \tag{5.8}$$

Finally, the overall spatial selectivity index (S) was calculated as the average of the individual selectivity indices of all six channels:

$$S = \frac{1}{6}\sum_{i=1}^{6} S_i \,. \tag{5.9}$$

S ranges from 0 to 100%, with zero corresponding to no spatial selectivity and 100% to the maximum achievable selectivity.

5.1.4.3 Percent Crosstalk

To quantitatively evaluate the separation of the neural patterns, a measure of crosstalk was defined for channel i as:

$$PercentCrosstalk_i = \frac{E[(y_i - s_i)^2]}{E[s_i^2]} \quad (\%), \tag{5.10}$$

where y_i is the i_{th} output neural pattern, and s_i is the i_{th} source pattern. Based on this definition, the smaller the percent crosstalk, the better the separation due to the smaller difference between the source and the corresponding output signal.

5.2 Results

For a total of sixty-six source signals in the eleven data sets, the mean SNR was measured as 0.43 ± 0.19 (or –8.14 ± 3.75 dB). Figure 5.4 is the raw signals of the source patterns of an example data set, where the motor signals are entirely obscured by the sensory neural activity due to the low SNR. The SNRs of the six channels shown in Figure 5.4 were 0.51, 0.55, 0.60, 0.44, 0.34, and 0.60 respectively with a mean SNR of 0.51 (or –5.85 dB). The stimulus-trigger averaged version of the source patterns are shown in Figure 5.5.

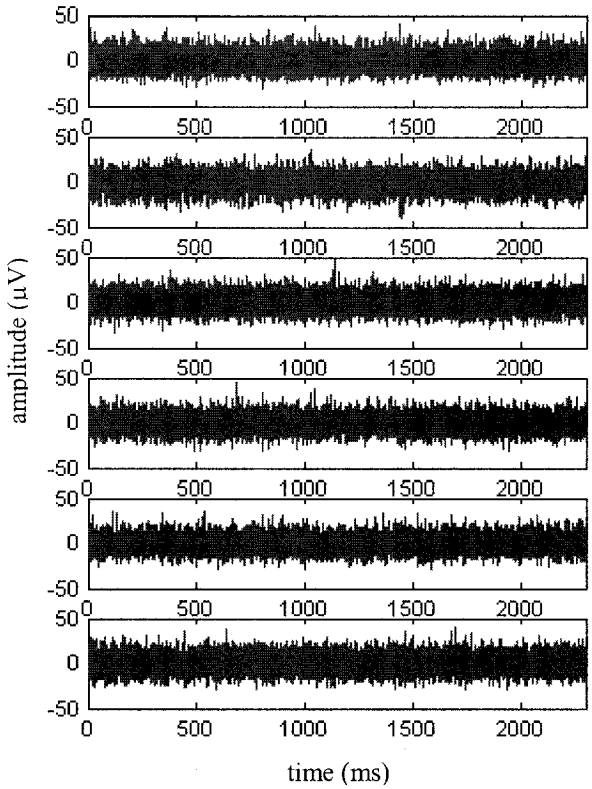

Figure 5.4 256 consecutive acquisitions of six neural patterns before averaging (with stimulus artifacts removed).

The simulated six-contact neural recording was obtained by multiplying the source patterns with the mixing matrix $\boldsymbol{A}$. Figure 5.6 shows the *averaged* version of the simulated neural recordings. Since the initial spatial selectivity was chosen to be only 1% by the matrix $\boldsymbol{A}$, the signals look very much alike in time.

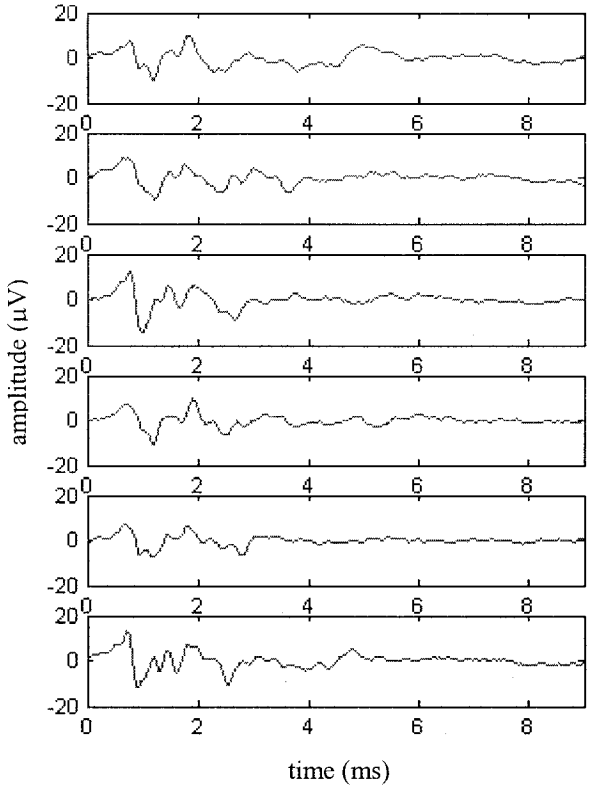

Figure 5.5 Stimulus-trigger averaged source patterns.

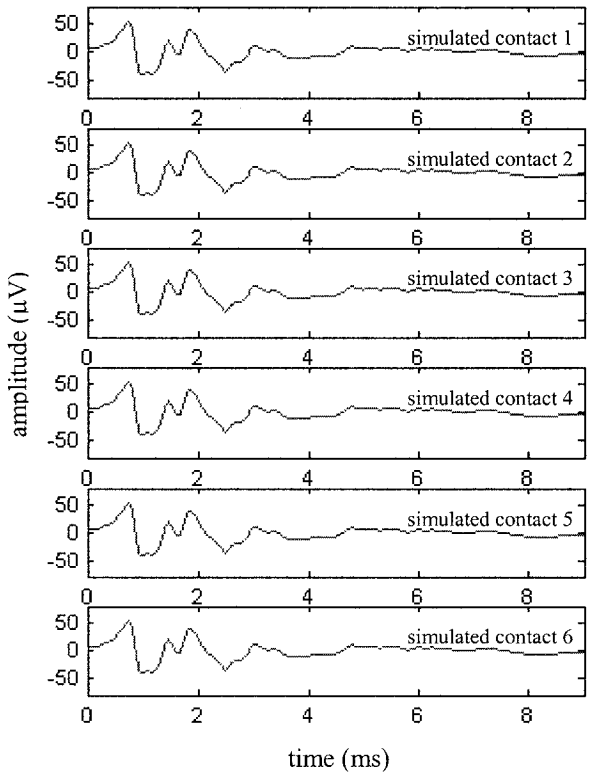

Figure 5.6 Averaged version of the simulated multi-contact neural recordings.

The signals in Figure 5.4, which was the *unaveraged* version of the neural recordings shown in Figure 5.6, was applied as input to the BSS neural network for separation. In this data set, the initial learning rate $\mu(0)$ was set to be 0.00005 in the search phase of learning, and after $t_0 = 45500$ iterations $\mu(t)$ was exponentially decreased to zero in the convergence phase according to the equation:

$$\mu(t) = \mu(0) \times e^{-0.00008 \times (t - t_0)}. \tag{5.11}$$

The learning trajectories of the neural network coefficients $\boldsymbol{W}$ are shown in Figure 5.7. The coefficients converge to a stable point within a second. Figure 5.8 shows the *averaged* version of the output signals of the BSS neural network. The first 156 acquisitions of the output, during which the neural network was still converging, were not used, and only the last 100 acquisitions were averaged for each output channel.

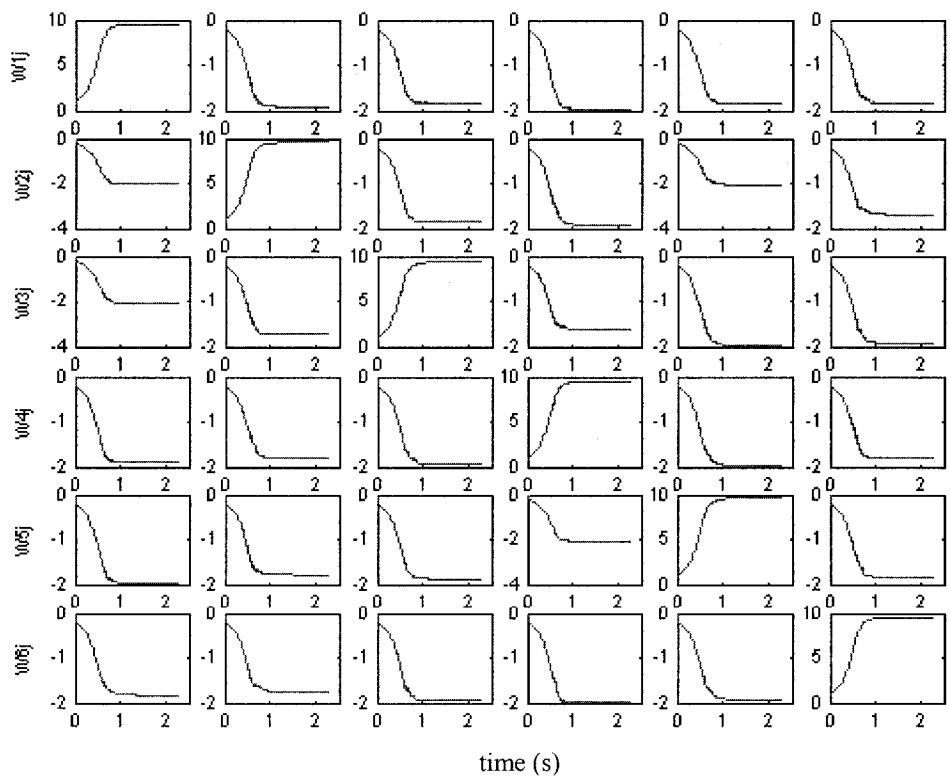

Figure 5.7 Learning trajectory of the BSS neural network coefficients ($\boldsymbol{W}$) of the first data set, showing convergence.

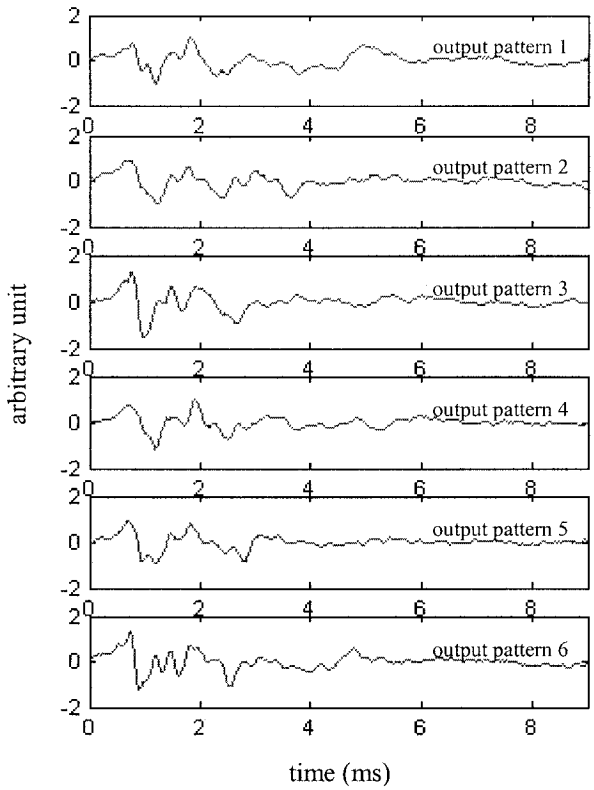

Figure 5.8 Neural patterns at the BSS neural network output.

Table 5.1 shows the percent crosstalk measurements of all the eleven data sets. The minimum and maximum crosstalk values in each data set are shown in bold. The first data set is the example set shown in Figures 5.4 to 5.8. Comparing the averaged version of the source patterns (Figure 5.5) and the output patterns (Figure 5.8), we concluded that the source patterns were recovered with a small percent crosstalk at the output of the BSS neural network.

Among the eleven data sets, the smallest percent crosstalk, 0.02%, occurs in data set 9, and the largest crosstalk, 6.41%, in data set 6. The average of the minimum crosstalks in all eleven data sets is 0.12%, and the average of the maxima is 2.51%.

Table 5.1 The percent crosstalk measurements.

Data Set	Percent Crosstalk (%)					
	Channel #1	**Channel #2**	**Channel #3**	**Channel #4**	**Channel #5**	**Channel #6**
1	0.14	0.16	0.11	**0.07**	**0.45**	0.43
2	1.04	0.73	**0.19**	0.74	**1.57**	0.81
3	0.24	1.46	0.61	**1.54**	**0.05**	0.82
4	**0.11**	1.27	0.85	0.15	0.80	**1.66**
5	2.19	0.90	0.56	**0.10**	0.15	**2.32**
6	0.92	**0.15**	0.75	***6.41***	0.27	4.04
7	0.69	**0.13**	0.96	0.24	0.21	**2.31**
8	**0.14**	**2.94**	0.25	0.63	2.24	2.21
9	**0.24**	***0.02***	***0.02***	0.05	0.21	0.12
10	0.95	**4.70**	3.78	**0.16**	1.55	4.68
11	2.70	2.47	**0.18**	**3.49**	1.05	0.73

5.3 Discussion

In this study, the single-layer feed-forward neural network model proposed by Cichocki and Unbehauen [72] was applied to separate the simulated multi-channel neural recordings from the spinal cord. Extensive computer simulations done by Cichocki and Unbehauen showed that the feed-forward structure was temporally stable independent of the initial conditions [72]. To ensure stability, the learning rate $\mu(t)$ must be upper-bounded to small values [97].

There is an inherent self-adaptive gain control mechanism in the learning rule due to the diagonal matrix $\boldsymbol{\Lambda} = diag\{\lambda_1, \lambda_2, ..., \lambda_n\}$ with the amplitude-scaling factor λ. We chose $\boldsymbol{\Lambda} = \boldsymbol{I}$ to obtain self-normalization of the output signals with energy being one. A variety of odd functions can be used as the activation functions. We applied various activation functions suggested by Cichocki and Unbehauen [72] and the results showed similar separation.

In a preliminary study, we obtained very good separation using the same BSS algorithm on simulated data of two-channel neural recordings [98]. The results showed very good separation of the two neural patterns with an improvement of the spatial selectivity from an initial value of less than 1% to 91%, despite the fact that the SNR of the signals was as low as 0.46 on average. The results of both the preliminary and this study demonstrate the effectiveness of the BSS technique in separating the neural channels in multi-contact recordings by taking advantage of spatial selectivity. Since the BSS algorithm does not require storing the input data, a real-time implementation of this separation method is feasible.

Finally, the epidural recordings from the SCI patients will not have sensory components since the sensory pathways are severed by the injury. The neural recordings from the proximal spinal cord of SCI patients will contain only the motor activity and thermal noise. This fact would increase the SNR of the spinal cord signals and thereby make it easier for the neural network to converge to a stable point.

CHAPTER 6

SEPARATION OF SPINAL CORD MOTOR SIGNALS USING FASTICA ALGORITHM

6.1 Methods

6.1.1 Data Collection

The data used in this chapter are the same as in Chapter 5. See "Data Collection" of Chapter 5 for details.

6.1.2 Data Analysis

6.1.2.1 Definition of Trials, Recordings, and Acquisitions

Seven *trials* were included in this study. Here "trial" means a specific implantation of the electrodes on the spinal cord. Multiple trials were made in a given cat and in each trial a set of *recordings* was obtained by stimulating various cortical points. Each electrode had multiple contacts (7 or 8), and each recording consisted of 256 *acquisitions* of 10 ms long neural signals following the cortical stimulus delivered at a rate of 2 pulses/sec.

6.1.2.2 Data Preprocessing Using PCA

PCA was used to estimate the dimensionality of the neural sources inside the LCST. The results of PCA revealed that only one *primary neural source* predominated, i.e., the eigenvalues of other principal components were relatively much smaller (the

eigenvalues of the second largest components were only 9.44 ± 5.36% of that of the predominant component).

Each recording lasted 128 seconds (256 acquisitions obtained at a stimulus rate of 2 pulses/sec). In order to test the temporal and spatial stability of the primary neural source during the stimulation of a single cortical point, the 256 acquisitions were divided into four equal *segments*. The 64 acquisitions of each segment were then stimulus-trigger averaged to extract the motor component in the presence of a large background noise (see Figure 5.2 for illustration of the raw and averaged signals).

The envisioned paradigm for the locations of the independent neural sources inside the white matter is shown in Figure 6.1. One primary neural source (large filled circle) and a few secondary sources (small circles) are depicted. These neural signals project to the spinal cord surface so that the recorded signal from each contact is a linear mixture of the projected signals from all the sources. The following linear mixture model describes the system:

$$x(t) = As(t), \tag{6.1}$$

where $x(t)$ are the neural recordings from the multi-contact surface electrode, and $s(t)$ are the independent neural sources. A is the unknown mixing matrix which depends on the volume conductor characteristics. The coefficients of A represent the relative projection strengths and polarities from the neural sources to the recording points (contacts) on the spinal cord surface.

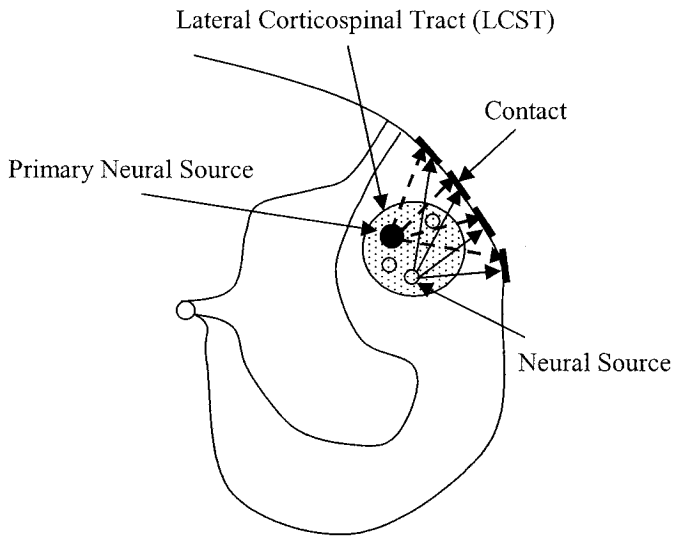

Figure 6.1 A depiction of the neural sources inside the lateral corticospinal tract (dotted area) and how they superimpose at the recording contacts.

6.1.2.3 Separation of Independent Sources Using FastICA Algorithm

The fixed-point FastICA algorithm [77] was applied to separate the mixed signals into independent source signals. Figure 6.2 is the block diagram of how the FastICA algorithm was performed to estimate the source signals from the observed multi-contact neural recordings. From 7 or 8 contacts in each recording, a reduced set of 4-contact recording was centered by subtracting the sample mean and used for analysis. Then the *stimulus-trigger averaged signal* $x(t)$ was fed into the FastICA algorithm to be separated. Since the first millisecond of each acquisition was discarded to eliminate the stimulus artifact, the averaged signal $x(t)$ was 9 ms long and contained 720 data points at a sampling frequency of 80,000 Hz.

At the output of the algorithm, the estimated independent sources $\hat{s}(t)$ are shown as:

$$\hat{s}(t) = Wx(t), \tag{6.2}$$

where W is the de-mixing matrix. Derived from equations (6.1) and (6.2), W is the inverse of the mixing matrix A, i.e.:

$$W = A^{-1}. \tag{6.3}$$

Out of 89 recordings, 64 (71.91%) reached convergence in all of the four segments. These data were included in the study.

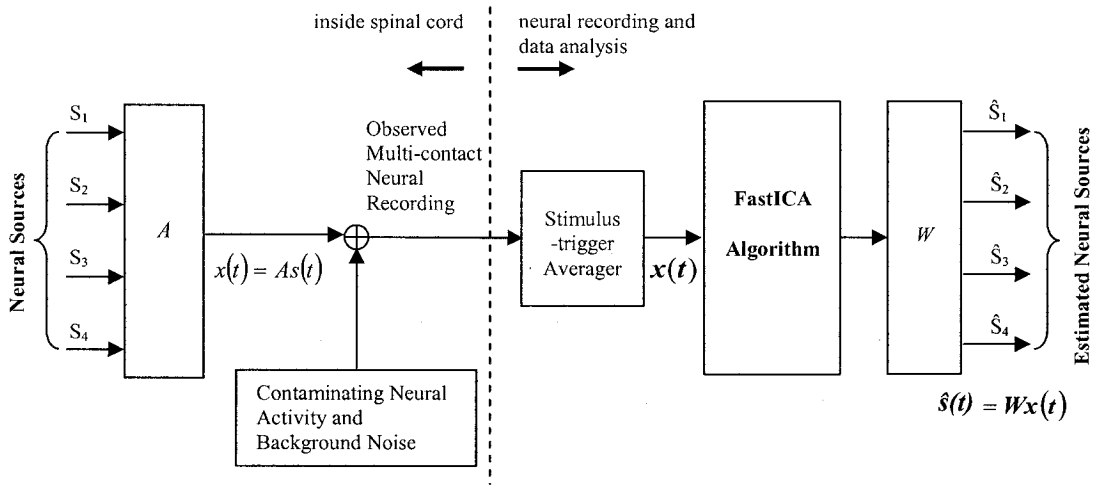

Figure 6.2 The block diagram of how the FastICA algorithm was applied to obtain the estimated source signals from the observed multi-contact neural recordings.

Each output channel represented an estimated neural source. The correlation operation between the estimated sources, $\hat{s}(t)$, and the mixed signals, $x(t)$, was performed to determine the primary neural source. The estimated source ($\hat{s}_i(t)$) that had the largest sum of the correlation coefficients (absolute value) with the mixed signals was considered as the primary source because it had the largest contribution to the mixture.

6.1.2.4 Statistical Analysis Based on MANOVA Test

During the 128-second stimulation process, the sources were assumed to move slowly within the white matter, indicated by the slight variations in the mixing matrix $\boldsymbol{A}$ across the four segments of each recording. To test if the primary neural source was relocating within the cord as a function of stimulation point in the cortex, and not so much within a recording, the multivariate analysis of variation (MANOVA) was performed. The MANOVA tests were applied both on the original signals (before FastICA) and the reconstructed primary source signals (after FastICA).

Before FastICA, MANOVA test was applied to the peak-to-peak measurements of the first volley in the mixed signals recorded from the electrode contacts. After FastICA, the statistical analysis was applied to the peak-to-peak measurements of the first volley of the reconstructed primary source signals. The reconstructed primary signals were obtained by scaling the estimated primary source with the "*primary source column*" of $\boldsymbol{A}$. The primary source column is the column in $\boldsymbol{A}$ that corresponded to the projection from the primary neural source. The recordings in each trial were then clustered into groups of two, three, or four. Those recordings that had the largest distances between their primary sources were grouped together. The α values of MANOVA before and after FastICA were compared to see if the channel separation was improved by selecting the primary neural source and eliminating the secondary sources.

The same procedure of MANOVA tests were performed on the predominant principal component resulted from PCA to compare the separation performance of PCA and ICA on spinal cord neural recordings.

6.2 Results

Figure 6.3 shows an example of the averaged version of the 4-contact recording (mixed signal), which is the input to the FastICA algorithm, overlaid by the projections of the four sources that generate the mixture. Each projection is calculated by scaling the estimated independent source with the corresponding column of the mixing matrix $\boldsymbol{A}$. Table 6.1 shows the correlation coefficients between the mixture and the four contributing sources into each contact. The projections from the first separated source stand out having the largest correlation coefficients with the mixture for all the contacts. This source is the primary neural source. The variation analysis showed that the primary sources contained 74.51 ± 10.43% of the total energy of the mixed signals across all the data in this study. Due to the ambiguity of the order in which the output channels of the FastICA algorithm are arranged [99, 100], the primary neural source could occur in any output channel.

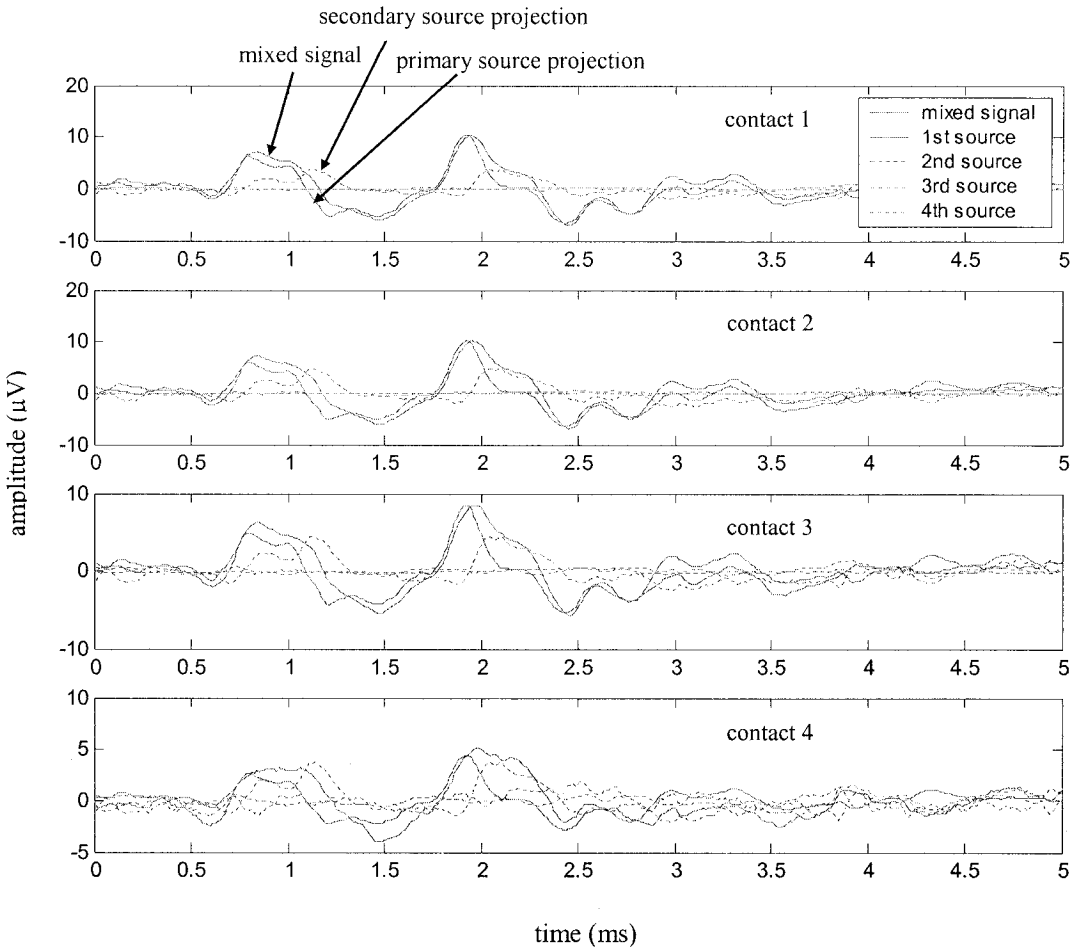

Figure 6.3 An example of the averaged version of the 4-contact recordings (mixed signals), overlaid by the projections of the four sources that generate the mixture.

Table 6.1 Correlation coefficients between the mixed signals and the reconstructed projections of the four separated sources for each contact.

Mixed Signals of	Projections from the Separated Sources			
	#1 *(Primary)*	#2	#3	#4
Contact #1	**0.9866**	0.0060	0.1588	0.0382
Contact #2	**0.9601**	0.0240	0.2736	0.0521
Contact #3	**0.9340**	0.0278	0.3485	0.0739
Contact #4	**0.6417**	0.5730	0.5098	0.0042

Figure 6.4 is the plot of the "primary source column" of the mixing matrix $\boldsymbol{A}$ for three recordings in a trial. For each recording, the mean and the standard deviation of the coefficients across the four segments are plotted. Y-axis represents the projection strength of the primary source to the contact. The contact number is indicated by the X-axis. The standard deviation bars indicate how much variation takes place across the four segments during a 128-second recording. The α value of the MANOVA test was 0.8392 for the mixture, and 0.7491 after FastICA. Each plot is shifted slightly in horizontal direction for clarity of the figure.

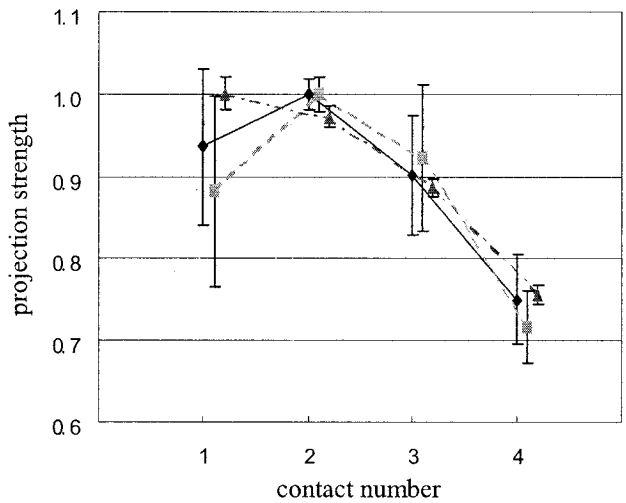

Figure 6.4 The plot of the "primary source column" of mixing matrix $\boldsymbol{A}$ of three recordings of an example trial. Each plot is shifted slightly to the right for clarity of the figure.

The fact that the mean projection strengths vary between recordings indicates that the source is relocating in the spinal cord as the stimulation point in the cortex is moving. In order to find out if this relocation is significant compared to the random walking of the source during stimulation of one cortical point, the analysis of variance was applied. The recordings were clustered into two, three or four subgroups based on the results of

MANOVA test as described before. The subgroups were chosen to minimize the α value, indicating the largest separation of signals.

Alpha values of the MANOVA test are listed in Table 6.2 for original signals (mixed), after FastICA and after PCA processes. A varying number of recordings converged in each trial during the application of the FastICA algorithm. It can be concluded from these α values that in a trial, there were at least a few spatially separated primary neural sources (or fiber groups that carried neural signals from the motor cortex) during stimulation of different points in the motor cortex. Compared with the original signals, the α value decreases in all cases as a result of the FastICA algorithm (except for the first trial, shown as bold numbers), indicating that the channel separation was improved when the primary source was taken and the secondary ones were dropped from the analysis.

The α values after FastICA are always smaller than that of following the PCA, except for one case (second line in the table). In most cases (shown as italic bold numbers), the PCA did not improve the channel separation of the original signal, indicated by an increase in the α values.

Therefore, elimination of the contributions made by the secondary sources into the mixed signals increased the distinguishability of the primary sources associated with different cortical stimulation points. Comparison between ICA and PCA reveals that ICA performs better in this application.

Table 6.2 Alpha values of the MANOVA test.

Trial No.	Cat No.	Electrode Design	Implant Site and Method	No. of Converging Recordings	No. of Sub-groups	α of MANOVA Test		
						Original Signal	After FastICA	After PCA
1	1	1	C5/C6 epidurally, right	3 of 9	2	0.0047	**0.0339**	***0.0737***
					3	0.1595	**0.8214**	0.0737
2	1	2	C5/C6 epidurally, left	6 of 8	2	0.0587	0.0005	0.0421
					3	0.1357	0.0278	***0.2293***
					4	0.1638	0.1164	***0.2293***
3	1	2	C5/C6 intradurally, left	3 of 3	2	0.2060	0.0243	***0.4067***
					3	0.4252	0.1134	***0.5351***
4	1	2	C5/C6 intradurally, left (repeat)	9 of 9	2	0.0015	0.0001	***0.0180***
					3	0.0241	0.0017	***0.0964***
					4	0.1478	0.0056	0.0426
5	2	3	C5/C7 epidurally, left	5 of 13	2	0.4795	0.0028	0.0934
					3	0.4795	0.0421	***0.4948***
					4	0.5247	0.4099	***0.9258***
6	3	3	C4/C6 epidurally, left	22 of 26	2	0.2342	0.0001	0.0221
					3	0.2590	0.0010	***0.2693***
					4	0.3388	0.0098	***0.9787***
7	4	3	C4/C6 epidurally, left	16 of 21	2	0.2845	0.0001	0.1432
					3	0.3931	0.0012	***0.5879***
					4	0.4266	0.0021	***0.5879***

6.3 Discussion

In Chapter 5, an adaptive BSS algorithm [72] was tested with simulated six-channel spinal cord recordings, and percent crosstalk was used as a measure for the channel separation performance. The performance of adaptive learning depends on a good choice of the parameters in the learning rule, such as the initial learning rate and the exponential coefficient of the decreasing learning rate in the convergence phase. The results of Chapter 5 showed that perfect separation could be achieved when the parameters of the learning rule were chosen properly.

In this Chapter, the fixed-point FastICA algorithm was applied to improve the channel separation of spinal cord surface recordings. There were 7 or 8 contacts (channels) in each recording, and different numbers of contacts were tested for best

separation. Some of the contacts were excluded from analysis because of a large stimulation artifact or excessive noise in the recording. A trade-off existed between the convergence speed of the FastICA algorithm and the number of input channels. Multiple trials indicated that decreasing the number of channels made the algorithm easier to converge. Four was chosen as the number of input channels to include the maximum amount of data in the analysis while having a stable convergence. The algorithm did not converge in a few cases. This may be due to the nature of the neural data, i.e., the neural sources were not mutually independent.

Unlike in the adaptive learning algorithms, the computations of the FastICA algorithm were made in batch mode, i.e., a certain number of data points were used in a single step (720 data points in this study). The convergence is slow with the adaptive learning algorithms, whereas the fixed-point iteration algorithm has very fast and reliable convergence. Although the FastICA is non-adaptive, it has advantages of neural algorithms; i.e., it is parallel, distributed, computationally simple, and requires little memory space [77]. The stochastic gradient methods are more suitable for fast changing environment, while fixed-point algorithm's appealing convergence properties make it a very good choice in an environment where fast real-time adaptation is not necessary. We used the fixed-point FastICA algorithm assuming that the neural source locations in the spinal cord will be reproducible for the same cortical points. Therefore, the $\boldsymbol{A}$ matrix will be constant over time.

Unlike the study in Chapter 5, where the recordings were artificially mixed by taking the weighted sum of multiple neural patterns, naturally mixed multi-contact recordings were used in this Chapter. The mixing of neural sources occurred in the

volume conductor of the spinal cord while the projections were recorded from the surface (Figure 6.1). Therefore, we do not have access to the neural sources, which makes it difficult to validate the assumptions made about the sources for carrying out ICA. This problem is very common in the application of ICA method on biomedical signals. Some of these assumptions were tested as follows.

First, for the real multi-contact spinal cord recordings, PCA revealed that most of the variation in the data came from a single neural source, which is the "primary neural source". There were still other secondary, smaller sources that made the location of the primary sources more 'fuzzy' in the multidimensional space. The plot of the "primary source column" of A (Figure 6.4) confirmed that the projection coefficients of the primary neural source remained almost the same across the four data segments in time. In other words, the primary neural source was temporally and spatially stationary (with slight relocation of the source in time).

Second, since the assumption of the mutual independence of the unknown neural sources can not be tested, the correlation coefficients between each pair of the estimated sources were calculated instead. The results were nearly zero (2.2812E-14 ± 1.9837E-14), indicating mutual uncorrelatedness of the estimated neural sources. On the contrary, the correlation coefficients between each pair of the mixed signals were close to one (0.8686 ± 0.0554), indicating that the mixed signals were nearly fully correlated.

Third, another important assumption about the sources, the probability distribution function, was considered. The mixture of multiple non-gaussian sources can appear normally distributed [65]. Normal plot and K-S test tools were applied to test the nongaussianity of the estimated sources. The results showed that in each recording, the

primary source had non-gaussian distribution. The other three sources were always non-gaussian distributed, with rare cases where one source appeared close to gaussian (K-S test could not reject the null hypothesis at $\alpha = 0.05$). However, the ICA still converged when only one of the independent components was gaussian [71]. The mixed signals were tested as non-gaussian distributed as well. Furthermore, the kurtosis measurements of the mixed signals and the estimated sources were compared since maximizing the nongaussianity is one of the characteristic outcomes of ICA when the signals are successfully separated. The results showed that the absolute values of the kurtosis of the mixed signals (2.9654 ± 1.9273) were always smaller than that of the estimated sources (3.5563 ± 1.3034), indicating that the mixed signals was more gaussian than the estimated sources.

PCA is a classical statistical method which has been widely used in data analysis and compression. The main difference between PCA and ICA is that PCA only uses the 2^{nd} order statistics, while ICA imposes statistical independence on higher-order statistics [62]. Therefore, PCA only ensures that the output channels are *uncorrelated*, while ICA ensures that the output paris are *independent*. In our case, the ICA takes advantage of the randomness introduced into the signals by variations in the nervous system, which makes the sources more independent of each other. The results of this study demonstrate that FastICA algorithm is effective in increasing the channel separation of spinal cord recordings by eliminating the secondary neural sources, while PCA does not improve the channel separation.

The BSS technique can be the method of choice for improving the channel separation not only with surface recordings of the spinal cord but also for the whole nerve recordings in the peripheral nervous system [69].

CHAPTER 7

CONCLUSIONS AND FUTURE RESEARCH

7.1 Conclusions

The research work addressed in this dissertation contains the neuroscience and neural signal processing aspects for the development of spinal cord-computer interface (SCCI). This neural interface is developed to generate voluntary motor control signals for the individuals with SCI.

In the neuroscience aspect, which is the investigation of the organization in the white matter of the cervical spinal cord, the results suggest that there is a certain level of functional organization in the descending tracts of the dorsolateral funiculus at C5/C6 and C6/C7 segmental borders in the cat. The areas dedicated for various forelimb muscles were overlapping extensively. In general, the distal muscle maps were biased towards the ventro-lateral aspect of the funiculus, whereas the elbow muscle activation maps were spread to both dorsal and ventral sides. The elbow flexors were activated most readily in both segmental borders studied. In both segmental borders, the fibers in the middle of the dorsolateral funiculus had relatively higher thresholds. The evoked responses were generally not distinct, pure movements of individual forelimb segments (elbow flexion, etc). Direct stimulation of the descending tracts mostly generated short muscle twitches rather than sustained forces.

In the neural signal processing aspect, the feasibility of increasing the channel separation of spinal cord recordings was explored using the BSS technique. First, the BSS technique was tested for separation of neural patterns (channels) extracted from the recordings of the corticospinal tract and mixed artificially outside the spinal cord. The results demonstrate the effectiveness of the BSS algorithm for almost complete separation of simulated multi-channel spinal cord recordings with a very small initial spatial selectivity and SNR. Percent crosstalk is a convenient measure to assess the neural channel separation quantitatively.

Secondly, the FastICA algorithm was applied to real multi-channel spinal cord recordings to improve the channel separation by elimination of the secondary sources. Neural signals recorded with multi-contact surface electrodes were treated as a linear mixture of independent components generated by neural sources located inside the spinal cord. The channel separation was improved in all cases except one by the FastICA technique, indicated by a large decrease in the α parameter of MANOVA test. Comparison between ICA and PCA reveals that ICA is more suitable for the separation of spinal cord neural recordings.

The results of this analysis support the conclusions of the previous work [37] that the cortical points can be distinguished based on the location of the neural signals inside the spinal cord. This result suggests that a multi-channel SCCI for individuals with SCI may be feasible. The information rate of such an interface can be improved by applying the FastICA method to the recorded signals.

7.2 Future Research

This dissertation constitutes the first aim of the project "Extraction of Motor Signals from the Spinal Cord". Based on the results from the acute animal experiments, a certain level of functional organization was revealed to exist in the descending tracts of the cervical spinal cord. The next step is to study the organization in the descending tracts in freely moving animals using chronic recording techniques. The animals will be chronically implanted with microelectrode arrays during a reproducible behavior. The study on chronic spinal cord recordings may lead to the discovery of some natural activation pattern of the descending tracts. The quality and long-term stability of these signals will be studied.

The spinal cord recordings acquired while the animals are performing a behavioral task will be analyzed to extract multi-channel motor signals. The BSS technique is expected to be effective in improving the channel separation of the chronic spinal cord recordings. Then the extracted motor signals will be analyzed to generate voluntary motor control signals using linear and non-linear signal processing techniques. This kind of signals could be used to control neural prostheses or assistive devices for the quadriplegic individuals.

The information rate is an important parameter of the neural interfaces. The higher the information rate, the faster the speed with which the voluntary motor control signals could be generated by the interface. This dissertation studies the feasibility of applying the BSS method to improve the channel separation of multi-channel spinal cord recordings. Further studies could be performed on the signals generated by other neural interfaces, such as the brain-computer interface (BCI), to investigate the effectiveness of

the BSS technique in improving the information rate not only for spinal cord interface but also for other neural interfaces being developed.

APPENDIX A

STIMULATION AND DATA ACQUISITION SOFTWARE DEVELOPED USING LABVIEW

1. Front panel for input of parameters of stimulation and data acquisition.

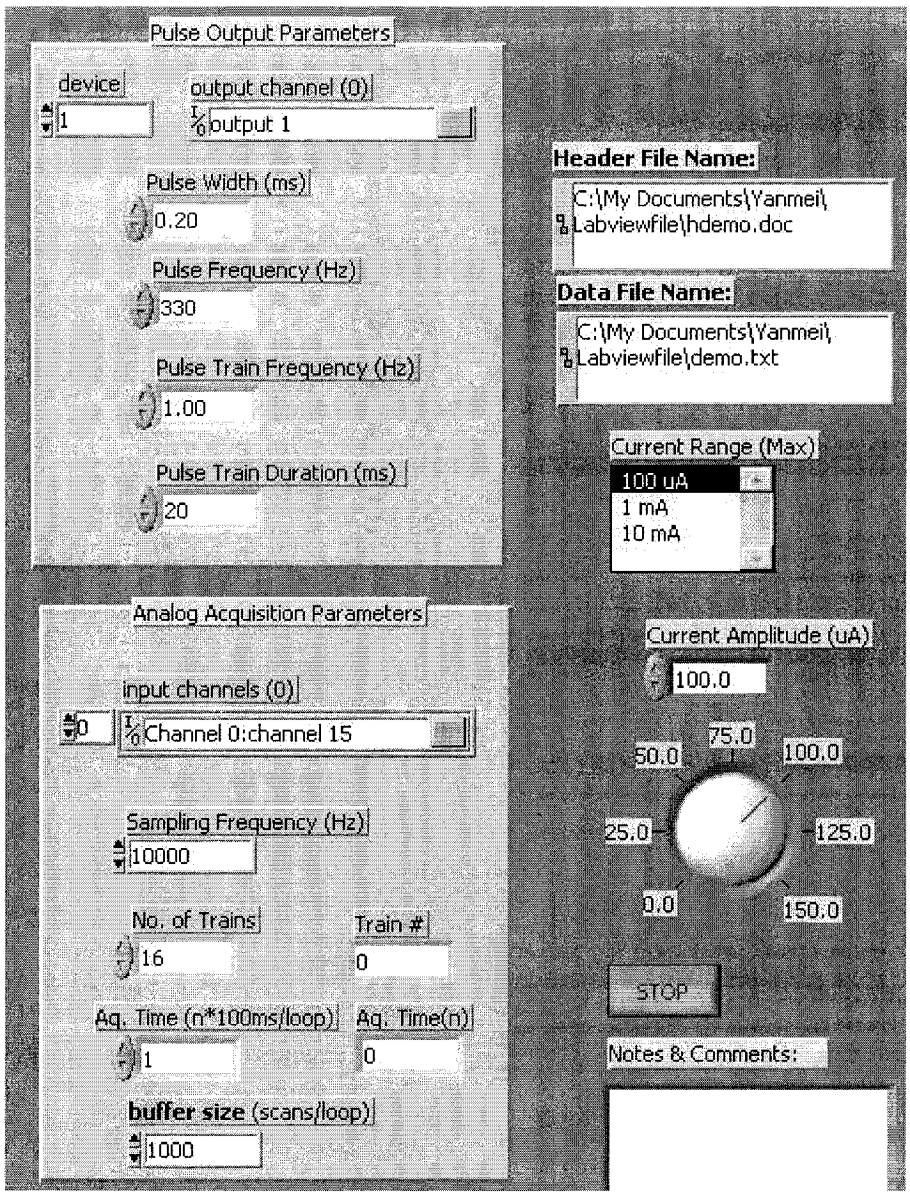

2. Front panel for input of parameters of stimulus waveform and its display.

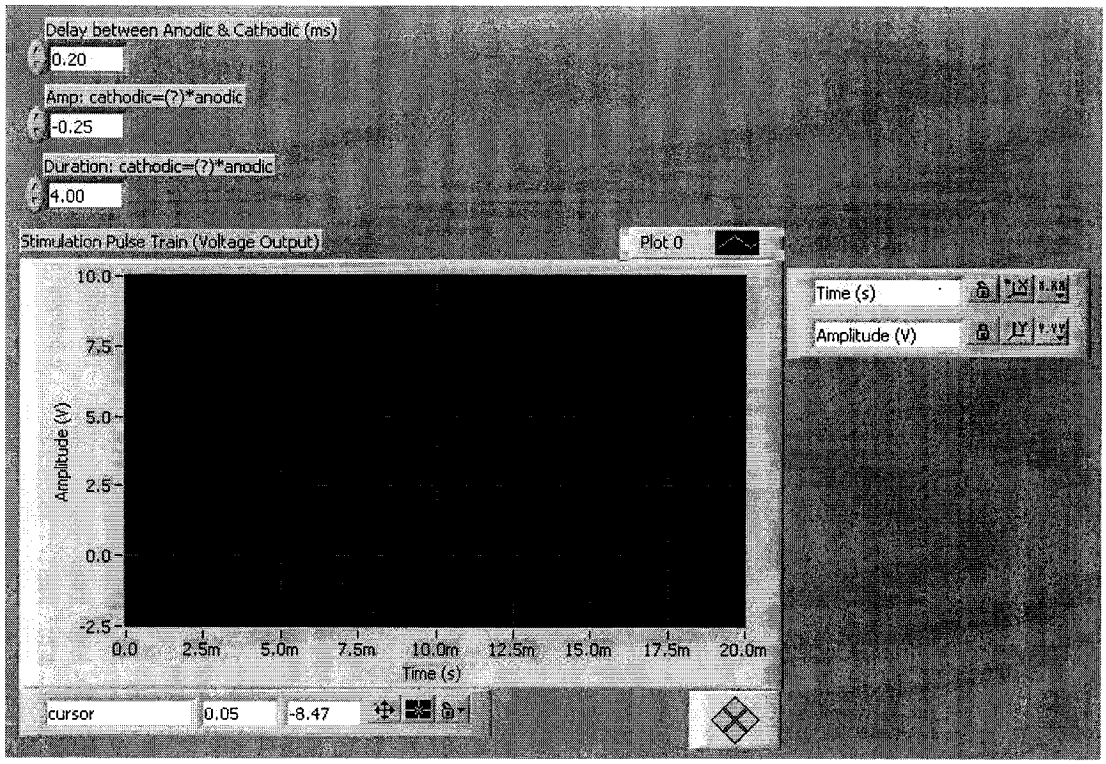

3. Front panel for display of real-time or averaged 16-channel analog input of EMG activities.

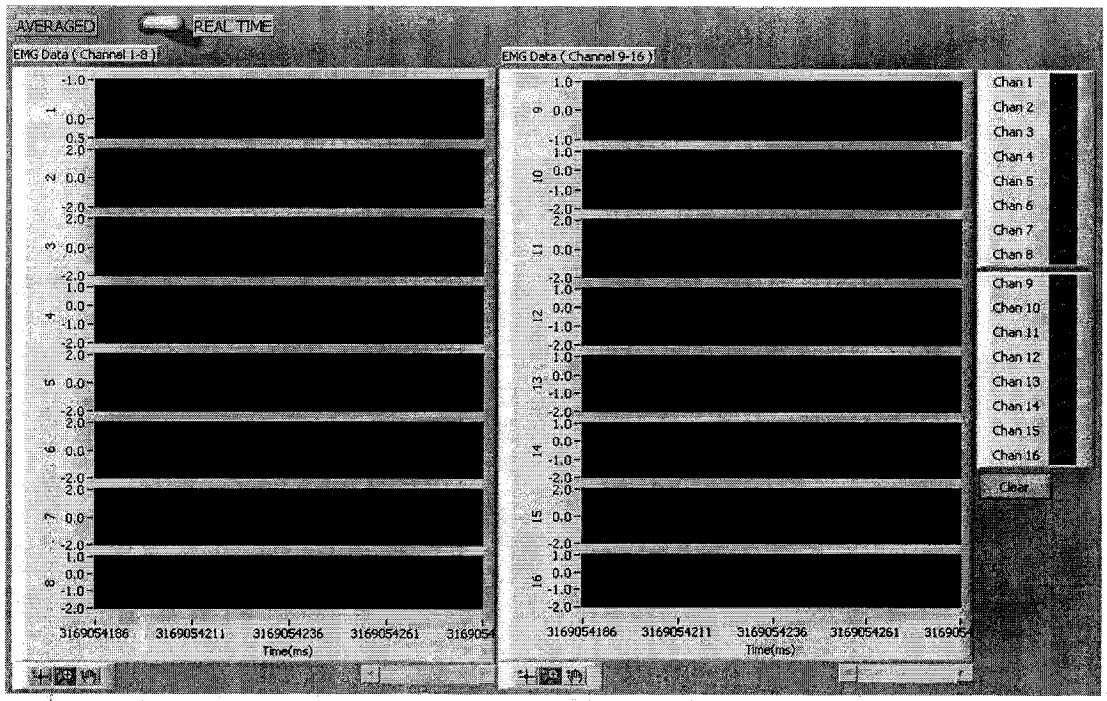

APPENDIX B

FLOWCHART OF EMG RESPPONSE ANALYSIS

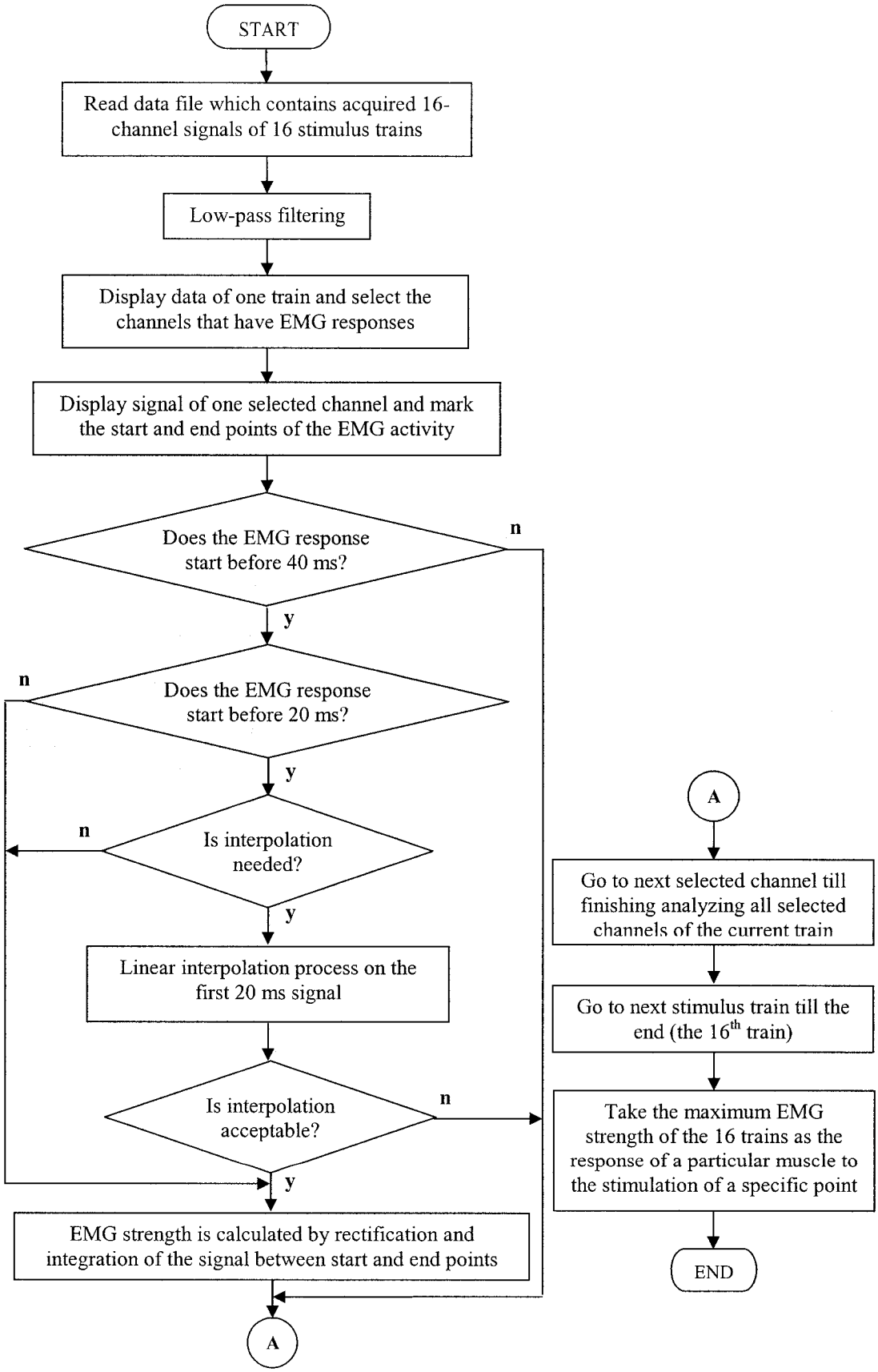

REFERENCES

1. Spinal Cord Injury: facts and figures at a glance. http://www.spinalcord.uab.edu, August 2004.

2. Factsheet #5: What's new in Spinal Cord Injury treatment and cure research? *National Spinal Cord Injury Association Resource Center*, http://www.makoa.org/nscia/fact05.html

3. P. H. Peckham, M. W. Keith, K. L. Kilgore, J. H. Grill, K. S. Wuolle, G. B. Thrope, P. Gorman, J. Hobby, M. J. Mulcahey, S. Carroll, V. R. Hentz, and A. Wiegner, "Efficacy of an implanted neuroprosthesis for restoring hand grasp in tetraplegia: a multicenter study," *Archives of Physical Medicine and Rehabilitation*, vol. 82, no. 10, pp. 1380-1388, 2001.

4. R. T. Lauer, P. H. Peckham, and K. L. Kilgore, "EEG-based control of a hand grasp neuroprosthesis," *NeuroReport*, vol. 10, pp. 1767-1771, 1999.

5. http://www.sigmedics.com/TheParastep/theparastep.html

6. New neural prosthesis can restore movement to paralyzed limbs, http://www.cwru.edu/pubs/cnews/1997/9-4/freehand.htm

7. J. R. Wolpaw and D. J. McFarland, "Multichannel EEG-based brain-computer communication," *Electroencephalography and Clinical Neurophysiology,* vol. 90, no. 6, pp. 444-449, 1994.

8. J. R. Wolpaw and D. J. McFarland, "Control of a two-dimensional movement signal by a non-invasive brain-computer interface in humans," *Proceedings of the National Academy of Sciences of the United States of America,* vol. 101, no. 51, pp. 17849-17854, 2004.

9. L. A. Farwell and E. Donchin, "Talking off the top of your head: A mental prosthesis utilizing event-related brain potentials," *Electroencephalography and Clinical Neurophysiology,* vol. 70, no. 6, pp. 510-23, 1988.

10. E. Donchin, K. M. Spencer, and R. Wijesinghe, "The mental prosthesis: Assessing the speed of a P300-based brain computer interface," *IEEE Transactions on Rehabilitation Engineering,* vol. 8, no. 2, pp. 174-179, 2000.

11. J. R. Wolpaw, N. Birbaumer, D. J. McFarland, G. Pfurtscheller, and T. M. Vaughan, "Brain-computer interfaces for communication and control," *Clin. Neurophysiol.*, vol. 113, pp. 767-791, 2001.

12. J. R. Wolpaw, N, Birbaumer, W. J. Heetderks, D. J. McFarland, P. H. Peckham, G. Schalk, E. Donchin, L. A. Quatrano, C. J. Robinson, and T. M. Vaughan, "Brain-computer interface technology: a review of the first international meeting," *IEEE Transactions on Rehabilitation Engineering*, vol. 8, no. 2, pp. 164-173, 2000.

13. J. M. Carmena, M. A. Lebedev, R. E. Crist, J. E. O'Doherty, D. M. Santucci, D. F. Dimitrov, P. G. Patil, C. S. Henriquez, M. A. L. Nicolelis, "Learning to control a brain-machine interface for reaching and grasping by primates," *PLoS Biology*, vol. 1, no. 2, pp. 193-208, 2003.

14. S. P. Levine, J. E. Huggins, S. L. BeMent, R. K. Kushwaha, L. A. Schuh, M. M. Rohde, E. A. Passaro, D. A. Ross K. V. Elisevich, and B. J. Smith, "A direct brain interface based on event-related potentials," *IEEE Transactions on Rehabilitation Engineering*, vol. 8, no. 2, pp. 180-185, 2000.

15. J. K. Chapin, K. A. Moxon, R. S. Markowitz, and M. A. L. Nicolelis, "Real-time control of a robot arm using simultaneously recorded neurons in the motor cortex," *Nature Neuroscience*, vol. 2, pp.664-670, 1999.

16. P. R. Kennedy and R. A. E. Bakay, "Restoration of neural output from a paralyzed patient using a direct brain connection," *NeuroReport*, vol. 9, pp. 1707-1711, 1998.

17. P. J. Rousche and R. A. Normann, "Chronic recording capability of the Utah Intracortical Electrode Array in cat sensory cortex," *Journal of Neuroscience Methods*, vol. 82, pp. 1-15, 1998.

18. P. R. Kennedy and R. A. E. Bakay, "Activation of single action potentials in monkey motor cortex during long-term task learning," *Brain Research*, pp. 251-254, 1997.

19. J. P. Donoghue, "Connecting cortex to machines: recent advances in brain interfaces," *Nature Neuroscience Supplement*, vol. 5, pp. 1085-1088, 2002.

20. M. D. Serruya, N. G. Hatsopoulos, L. Paninski, M. R. Fellows, and J. P. Donoghue, "Instant neural control of a movement signal," *Nature*, vol. 416, pp. 141-142, 2002.

21. D. M. Taylor, S. I. Tillery, and A. B. Schwartz, "Direct cortical control of 3D neuroprosthetic devices," *Science*, vol. 296, 1829-1832, 2002.

22. J. Wessberg, et al. "Real-time prediction of hand trajectory by ensembles of cortical neurons in primates," *Nature*, vol. 408, pp. 361-365, 2000.

23. A. Constans, "Mind over machines: Brain-machine interfaces help locked-in patients communicate and quadriplegics control their world," *The Scientist*, vol. 19, no. 3, pp. 27, 2005.

24. W. J. Levy and D. H. York, "Evoked potentials from the motor cortex in man," *Neurosurgery*, vol. 12, pp. 422-429, 1983.

25. R. Q. Cracco, V. E. Amassian, P. J. Maccabee, and J. B. Cracco, "Transcranial stimulation: technique and interpretation of the effects of stimulating motor and non-motor cortical regions in man," In: J. E. Desmedt (Ed), *Neuromonitoring in Surgery* (Amsterdam: Elsevier), pp. 61-69, 1989.

26. J. C. Rothwell, P. D. Thompson, B. L. Day, S. Body, and C. D. Marsden, "Stimulation of the human motor cortex through the scalp," *Exp. Physiol.*, vol. 76, pp. 169-200, 1991.

27. D. Burke, R. G. Hicks, and J. P. H. Stephen, "Corticospinal volleys evoked by anodal and cathodal stimulation of the human motor cortex," *J. Physiol.*, vol. 425, pp. 283-299, 1990.

28. D. Burke, R. Hicks, J. Stephen, I. Woodforth, and M. Crawford, "Assessment of corticospinal and somatosensory conduction simultaneously during scoliosis surgery," *Electroencephalography and clinical Neurophysiol.*, vol. 85, pp. 388-396, 1992.

29. A. Buss, K. Pech, D. Merkler, B. A. Kakulas, D. Martin, J. Schoenen, J. Noth, M. E. Schwab, and G. A. Brook, "Sequential loss of myelin proteins during Wallerian degeneration in the human spinal cord," *Brain*, vol. 128, no. 2, pp. 356-364, 2005.

30. K. Kalil, G. E. Schneider, "Retrograde cortical and axonal changes following lesions of the pyramidal tract," *Brain Res.*, vol. 89, pp. 15-27, 1975.

31. J. W. Lance, "Behavior of pyramidal axons after section," *Brain*, vol. 77, pp. 314-324, 1954.

32. A. M. Lassek, "The pyramidal tract: A study of retrograde degeneration in the monkey," *Arch. Neurol Psychiatry*, vol. 48, pp. 561-567, 1942.

33. S. P. Fishman, "Retrograde changes in the corticospinal tract of posttraumatic paraplegics," *Arch. Neurol.*, vol. 44, pp. 1082-1084, 1987.

34. R. Bronson, F. H. Gilles, J. Hall, and E. T. Hedley-Whyte, "Long term post-traumatic retrograde corticospinal degeneration in man", *Human Pathology*, vol. 9, no. 5, pp. 602-607, 1978.

35. M. F. Bear, B. W. Connors, M. A. Paradiso, *Neuroscience: Exploring the Brain (2nd edition)*, Lippincott Williams & Wilkins, 2000.

36. N. A. H. Dawnay and P. Glees, "Somatotopic analysis of fiber and terminal distribution in the primate corticospinal pathway," *Dev. Brain Res.*, vol. 26, pp. 115-123, 1986.

37. J. H. Martin, "Differential spinal projections from the forelimb areas of the rostral and caudal subregions of primary motor cortex in the cat," *Exp. Brain. Res.*, vol. 108, pp. 191-205, 1996.

38. G. E. Goode and D. E. Haines, "Origin, course, and termination of corticospinal fibers in a prosimian primate (Galago)," *Brain Behav. Evol.*, vol. 12, pp. 334-361, 1975

39. N. D. Jeffery and M. Fitzgerald, "Lack of topographical organization of the corticospinal tract in the cervical spinal cord of the adult rat," *Brain Res.*, vol. 833, pp. 315-318, 1999.

40. J. W. Barnard and C. N. Woolsey, "A study of localization in the corticospinal tracts of monkey and rat," *J. Comp. Neurol.*, vol. 105, pp. 25-50, 1956.

41. C. N. Liu and W. W. Chambers, "An experimental study of the cortico-spinal system in the monkey (Macaca Mulatta). The spinal pathways and preterminal distribution of degenerating fibers following discrete lesions of the pre- and postcentral gyri and bulbar pyramid," *J. Comp. Neur.*, vol. 123, pp. 257-283, 1964.

42. T. Drew and S. Rossignol, "Functional organization within the medullary reticular formation of intact unanesthetized cat. I. Movements evoked by microstimulation," *J. Neurophysiol.*, vol. 64, no. 3, pp. 767-781, 1990.

43. T. Drew and S. Rossignol, "Functional organization within the medullary reticular formation of intact unanesthetized cat. II. Electromyographic activity evoked by microstimulation," *J. Neurophysiol.*, vol. 64, no. 3, pp. 782-795, 1990.

44. A. Nieoullon and L. Raspel-Padel, "Somatotopic localization in cat motor cortex," *Brain Res.*, vol. 105, pp. 405-422, 1976.

45. A. P. Georgopoulos, M. R. DeLong, and M. D. Crutcher, "Relations between parameters of step-tracking movements and single cell discharge in the globus pallidus and subthalamic nucleus of the behaving monkey," *J. Neurosci.*, vol. 3, no. 8, pp. 1586-1598, 1983.

46. A. P. Georgopolous, J. Ashe, N. Smyrnis, and M. Taira, "Motor cortex and the coding of force," *Science*, vol. 256, pp. 1692-1695, 1992.

47. Y. Shinoda, T. Yamaguchi, and T. Futami, "Multiple axon collaterals of single corticospinal axons in the cat spinal cord," *J. Neurophysiol.*, vol. 55, no. 3, pp. 425-448, 1986.

48. B. Alstermak, H. Kummel, M. J. Pinter, and B. Tantisira, "Integration in descending motor pathways controlling the forelimb in the cat. 17. Axonal projection and termination of C3-C4 propriospinal neurons in the C6-Th1 segments," *Exp. Brain Res.*, vol. 81, pp. 447-461, 1990.

49. A. Canedo, "Primary motor cortex influences on the descending and ascending systems," *Progress in Neurobiol.*, vol. 51, pp. 287-335, 1997.

50. M. Sahin, "Selective recordings of motor signals from the corticospinal tract," *Proc. of Int. Functional Electrical Stimulation Society*, Cleveland, Ohio, USA, 2001.

51. M. Sahin, "Information capacity of the corticospinal tract recordings as a neural interface," *Annual of Biomedical Engineering*, vol. 32, no. 6, pp. 823-830, 2004.

52. Y. Chen, P. R. Christensen, K. D. Strange, and J. A. Hoffer, "Multi-channel Recordings from Peripheral Nerves: 2: Measurement of Selectivity," *Proc. of the Second Annual IFESS Conf. on Neural Prosthesis*, BC, Canada, 1997.

53. http://www.spinalinjury.net/html/_spinal_cord_101.html.

54. A. C. Guyton and J. E. Hall, *Textbook of Medical Physiology (10th edition)*, W. B. Saunders Company, 2000.

55. http://www.bio.davidson.edu/people/midorcas/animalphysiology/websites/2000/Rigel/Physiology.htm.

56. http://ivabs.massey.ac.nz/MUVSA/ass/phys/spine.htm.

57. http://education.yahoo.com/reference/gray/illustrations/figure?id=764.

58. T. Hongo, E. Jankowska, and A. Lundberg, "The rubrospinal tract. III. Effects on primary afferent terminals," *Experimental Brain Research*, vol. 15, pp. 39-53, 1972.

59. B. Alstermak, H. Kummel, M. J. Pinter, and B. Tantisira, "Integration in descending motor pathways controlling the forelimb in the cat. 17. Axonal projection and termination of C3-C4 propriospinal neurons in the C6-Th1 segments," *Experimental Brain Research*, vol. 81, pp. 447-461, 1990.

60. M. Illert, A. Lundberg, and R. Tanaka, "Integration in descending motor pathways controlling the forelimb in the cat. 3. Convergence on propriospinal neurones transmitting disynaptic excitation from the corticospinal tract and other descending tracts," *Exp. Brain Res.*, vol. 29, pp. 323-346, 1977.

61. M. Illert M, A. Lundberg, and R. Tanaka, "Integration in descending motor pathways controlling the forelimb in the cat. 2. Convergence on neurones mediating disynaptic cortico-motoneuronal excitation," *Exp. Brain Res.*, vol. 26, pp. 521-540, 1976.

62. S. Haykin (ed), *Unsupervised Adaptive Filtering. Volume 1: Blind Source Separation* (New York: John Wiley & Sons), 2000.

63. P. Comon, "Independent component analysis: a new concept?" *Signal Processing*, vol. 36, no. 3, pp. 287-314, 1994.

64. H. Liang, "Adaptive independent component analysis of multichannel electrogastrogram," *Medical Engineering & Physics*, vol. 23, pp. 91-97, 2001.

65. T.-P. Jung, S. Makeig, T.-W. Lee, M. J. McKeown, G. Brown, A. J. Bell, and T .J. Sejnowski, "Independent component analysis of biomedical signals," *The 2nd Int'l Workshop on Independent Component Analysis and Signal Separation*, pp. 633-644, 2002.

66. T.-P. Jung, C. Humphries, T.-W. Lee, S. Makeig, M. J. McKeown, V. Iragui, and T. J. Sejnowski, "Extended ICA removes artifacts from electroencephalographic recordings," *Advances in Neural Information Processing Systems*, vol. 10, pp. 894-900, 1998.

67. S. Makeig, M. Westerfield, T.-P. Jung, J. Covington, J. Townsend, T. J. Sejnowski, and E. Courchesne, "Functionally independent components of the late positive event-related potential during visual spatial attention," *Journal of Neuroscience*, vol. 19, no. 7, pp. 2665-2680, 1999.

68. M. J. McKeown, T.-P. Jung, S. Makeig, G. G. Brown, Kindermann, and T. J. Sejnowski, "Spatially independent activity patterns in functional magnetic resonance imaging data during the Stroop color-naming task," *Proc. of National Academy of Sciences of the United States of America*, vol. 95, no. 3, pp. 803-810, 1998.

69. J. Winter, M. Rahal, J. Taylor, and N. Donaldson, "Blind separation of EMG and ENG cuff electrode recordings," *Proc. of the 1999 IEEE Eng. in Med. and Bio. 21st Ann. Conf. and the 1999 Fall Meeting of the Biom. Eng. Soc. (1st Joint BMES / EMBS)*, pp. 581, Atlanta, Georgia, USA, 1999.

70. C. Jutten, and J. Herault, "Blind separation of sources, Part I: An adaptive algorithm based on neuromimetic architecture," *Signal Processing*, vol. 24, pp. 1-10, 1991.

71. A. Hyvärinen, and E. Oja, "Independent component analysis: Algorithms and applications," *Neural Networks*, vol. 13, no. 4, pp. 411-430, 2000.

72. A. Cichocki, and R. Unbehauen, "Robust neural networks with on-line learning for blind identification and blind separation of sources," *IEEE Transactions on Circuits*

and Systems - I: Fundamental Theory and Applications, vol. 43, no. 11, pp. 894-906, 1996.

73. P. Comon, "Blind separation of sources, Part II: Problems statement," *Signal Processing*, vol. 24, pp. 11-20, 1991.

74. E. Sorouchyari, "Blind separation of sources, Part III: Stability analysis," *Signal Processing*, vol. 24, pp. 21-29, 1991.

75. A. Cichocki, R. Unbehauen, and E. Rummert, "Robust learning algorithm for blind separation of signals," *Electronics Letters*, vol. 30, no. 17, pp. 1386-1387, 1994.

76. A. J. Bell, and T. J. Sejnowski, "An information maximization approach to blind separation and blind deconvolution," *Neural Computation*, vol. 7, no. 6, pp. 1129-1159, 1995.

77. A. Hyvärinen, "Fast and robust fixed-point algorithms for independent component analysis," *IEEE Transactions on Neural Networks*, vol. 10, no. 3, pp. 626-634, 1999.

78. X. Giannakopoulos, J. Karhunen, and E. Oja, "Experimental comparison of neural ICA algorithms," Proceeding of International Conference on Artificial Neural Network, pp. 651-656, Skövde, Sweden, 1998.

79. http://www.bio.psu.edu/faculty/strauss/anatomy/musc/forearmlat2.htm.

80. http://www.bio.psu.edu/faculty/strauss/anatomy/musc/forearmmed2.htm

81. Iridium Activation, http://www.engin.umich.edu/center/cnct/activ.html.

82. J. D. Weiland, D. J. Anderson, and M. S. Humayun, "*In vitro* electrical properties for iridium oxide versus titanium nitride stimulating electrodes," *IEEE Transactions on Biomedical Engineering*, vol. 49, no. 12, pp. 1574-1579, 2002.

83. L. S. Robblee, J. L. Lefko, and S. B. Brummer, "Activated Ir: An electrode suitable for reversible charge injection in saline solution," *J. Electrochem. Soc.*, vol. 130, pp. 731-733, 1983.

84. S. L. BeMent and J. B. Ranck, "A quantitative study of electrical stimulation of central myelinated fibers," *Exp. Neur.*, vol. 24, pp. 147-170, 1969.

85. D. M. Armstrong and T. Drew, "Forelimb Electromyographic responses to motor cortex stimulation during locomotion in the cat," *J. Physiol.*, vol. 367, pp. 327-351, 1985.

86. M. Illert, A. Lundberg, and R. Tanaka, "Integration in descending motor pathways controlling the forelimb in the cat. 1. Pyramidal effects on motoneurons," *Exp. Brain Res.*, vol. 26, pp. 509-519, 1976.

87. H. D. Patton and V. E. Amassian, *The Pyramidal Tract: Its Excitation and Functions* Handbook of Physiology ~ Neurophysiology II chapter 34 Univ. of Washington, Seattle pp. 837-861.

88. W. M. Landau, "Patterns of movement elicited by medullary pyramidal stimulation in the cat," *Electroencephal. and Clinical Neurophysiol.*, vol. 4, no. 4, pp. 527-546, 1952.

89. M. Illert, A. Lundberg, and R. Tanaka, "Integration in descending motor pathways controlling the forelimb in the cat. 3. Convergence on propriospinal neurones transmitting disynaptic excitation from the corticospinal tract and other descending tracts," *Exp. Brain Res.*, vol. 29, pp. 323-346, 1977.

90. M. Illert, A. Lundberg, Y. Padel, and R. Tanaka, "Integration in descending motor pathways controlling the forelimb in the cat. 5. Properties of and monosynaptic excitatory convergence on C3-C4 propriospinal neurones," *Exp. Brain Res.*, vol. 33, pp. 101-130, 1978.

91. M. Illert and S. Sasaki, "Integration in descending motor pathways controlling the forelimb in the cat. 15. Comparison of the projection from excitatory C3-C4 propriospinal neurones to different species of forelimb motoneurones," *Exp. Brain Res.*, vol. 63, pp. 543-556, 1986.

92. B. Alstermark and S. Sasaki, "Integration in descending motor pathways controlling the forelimb in the cat. 13. Corticospinal effects in shoulder, elbow, wrist, and digits motoneurons," *Exp. Brain Res.*, vol. 59, pp. 353-364, 1985.

93. D. M. Armstrong and T. Drew, "Electromyographic responses evoked in muscles of the forelimb by intracortical stimulation in the cat," *J. Physiol.*, vol. 367, pp. 309-326, 1985.

94. M. C. Tresch and E. Bizzi, "Responses to spinal microstimulation in the chronically spinalized rat and their relationship to spinal systems activated by low threshold cutaneous stimulation," *Exp. Brain Res.*, vol. 129, pp. 401-416, 1999.

95. H. Satomi, K. Takahashi, I. Kosaka, and M. Aoki, "Reappraisal of projection levels of corticospinal fibers in the cat, with special reference to the fibers descending through the dorsal funiculus: A WGA-HRP study," *Brain Res.*, vol. 492, pp. 255-260, 1989.

96. J. M. Brookhart, "A study of corticospinal activation of motor neurons," *Assoc. Res. In Nervous and Mental Disease*, vol. 30, pp. 157-173, 1952.

97. A. Cichocki and R. Unbehauen, *Neural Network of Optimization and Signal Processing*, (New York: Teubner-Wiley), pp. 461-471, 1994.

98. Y. Tie, and M. Sahin, "Separation of multi-channel spinal cord recordings using unsupervised adaptive filtering," *Proceeding of the Second Joint EMBS/BMES Conference*, pp. 2014-2015, Houston, Texas, USA 2014-2015, 2002.

99. A. Cichocki, and R. Unbehauen, *Neural Network for Optimization and Signal Processing* (New York: John Wiley & Sons), 1993.

100. L. Tong, R.-W. Liu, V. C. Soon, and Y.-F. Huang, "Indeterminacy and identifiability of blind identification," *IEEE Transactions on Circuits and Systems*, vol. 38, no. 5, pp. 499-509, 1991.